Recent Progress on Surface Reconstruction of Earth-Abundant Electrocatalysts for Water Oxidation

Yaoyao Li, Xinchuan Du, Jianwen Huang,* Chunyang Wu, Yinghui Sun, Guifu Zou, Chengtao Yang,* and Jie Xiong*

As one important electrode reaction in electrocatalytic and photoelectrochemical cells for renewable energy circulation, oxygen catalysis has attracted considerable research in developing efficient and cost-effective catalysts. Due to the inevitable formation of oxygenic intermediates on surface sites during the complex reaction steps, the surface structure dynamically evolves toward reaction-preferred active species. To date, transition metal compounds, here defined as TM-Xides, where "X" refers to typical nonmetal elements from group IIIA to VIA, including hydroxide as well, are reported as high-performance oxygen evolution reaction (OER) electrocatalysts. However, more studies observe at least exterior oxidation or amorphization of materials. Thus, whether the TM-Xides can be defined as OER catalysts deserves further discussion. This Review pays attention to recent progress on the surface reconstruction of TM-Xide OER electrocatalysts with an emphasis on the identification of the true active species for OER, and aims at disseminating the real contributors of OER performance, especially under long-duration electrocatalysis.

1. Introduction

Electrocatalytic water splitting for hydrogen generation is regarded as one of the most promising renewable energy technologies to convert solar energy into clean chemical fuel.[1] The whole water splitting contains two half electrode reactions: the hydrogen evolution reaction (HER) and the oxygen evolution reaction (OER).[2] Compared to two-electron HER, the four-electron OER with higher overpotential has been the main limiting factor to the efficiency improvement of electric energy conversion.[3]

The well-developed noble metal–based materials performed excellent OER activity but suffer from high cost and imperfect

Y. Li, X. Du, Dr. J. Huang, Dr. C. Wu, Prof. C. Yang, Prof. J. Xiong
State Key Laboratory of Electronic Thin Film and Integrated Devices
University of Electronic Science and Technology of China
Chengdu 610054, China
E-mail: huacrystalring@gmail.com; ctyang@uestc.edu.cn;
jiexiong@uestc.edu.cn
Prof. Y. Sun, Prof. G. Zou
Soochow Institute for Energy and Materials Innovations & Key Laboratory
of Advanced Carbon Materials and Wearable Energy Technologies of
Jiangsu Province
Soochow University
Suzhou 215006, China

stability, such like RuO_2/IrO_2. Since non-noble transition metals possess advantages of low cost, various oxidation states and ligands, considerable groups have developed earth-abundant materials for electrocatalytic OER. Here "X" refers to typical non-metal elements B, C, N, O, P, S, and Se from group IIIA to VIA, as well as hydro. Notably, the catalytic performance of these TM-Xides with the advantages of 3D structure even surpasses that of benchmark IrO_2 and RuO_2.[4] More than that, TM-Xides are further demonstrated to be bifunctional for both HER and OER. The stable long-time operation measurement without obvious performance decay completely demonstrates the advantages of corresponding materials.

However, in more cases, the surface reconstruction of post-OER (i.e., after OER reaction) catalysts is observed. As a result, what contributes to the activity of TM-Xides during OER electrolysis attracts more attention.[5] From the perspective of fact, it is necessary to make certain what is the real surface catalytic environment. Although there are lots of ex situ characterizations toward post-OER electrodes, the results may be inequable to the real case during catalysis.

Recently, various in situ characterizations are performed to identify the surface active species using Raman, X-ray photoelectron spectroscopy (XPS) and transition electron microscopy (TEM).[6] These operando techniques record the evolution of surface structure and investigate the phase transition process.[7] Thus the debate against the true OER catalysts tends to reach an acceptable and believable results. An understanding of the difference between electrochemical stability (described at a stable current or potential) and chemical stability (the material property) deserves a clear distinction. As Prof. Mullins and Prof. Jin pointed, the change of catalyst surface means the real identification of starting materials needs to be redefined.[8]

In this review, we will highlight the surface reconstruction of TM-Xides as OER catalysts and distinguish the chemical composition change hidden under long-time electrochemical stability. Corresponding modified electrochemical data are also discussed accompanied with the surface reconstruction to help determine the beneficial effects. Although there are cases describing the OER process without clear structure changes due to special structural effect, the general principles

ADVANCED
SCIENCE NEWS

www.advancedsciencenews.com

NANO · MICRO

small

www.small-journal.com

are in demand for further studies about OER electrocatalysis. A deeper understanding can help establish better standards for describing the OER activity of materials.

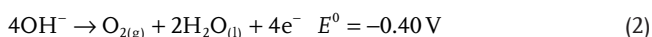## 2. OER Mechanism, Evaluation, and Surface Reconstruction

2.1. Mechanism

Oxygen evolution reaction is the anode reaction of overall water splitting. The reactions are different under acid and basic solutions (Equations (1) and (2), E^0 is the thermodynamic potential). Specific reaction processes involve some adsorption intermediates at catalytic sites, like OH*, OOH*, and O* both in acidic and alkaline conditions (Equations (3)–(10)).

Reaction in acidic solution

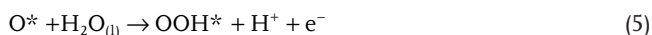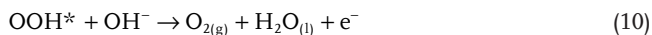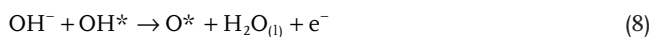$$2H_2O_{(l)} \rightarrow O_{2(g)} + 4H^+ + 4e^- \quad E^0 = -1.23\,V \tag{1}$$
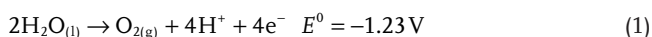
Reaction in basic solution

$$4OH^- \rightarrow O_{2(g)} + 2H_2O_{(l)} + 4e^- \quad E^0 = -0.40\,V \tag{2}$$

Four-electron process in acidic solution

$$H_2O_{(l)} \rightarrow OH^* + H^+ + e^- \tag{3}$$

$$OH^* \rightarrow O^* + H^+ + e^- \tag{4}$$

$$O^* + H_2O_{(l)} \rightarrow OOH^* + H^+ + e^- \tag{5}$$

$$OOH^* \rightarrow O_{2(g)} + H^+ + e^- \tag{6}$$

Four-electron process in basic solution

$$OH^- \rightarrow OH^* + e^- \tag{7}$$

$$OH^- + OH^* \rightarrow O^* + H_2O_{(l)} + e^- \tag{8}$$

$$O^* + OH^- \rightarrow OOH^* + e^- \tag{9}$$

$$OOH^* + OH^- \rightarrow O_{2(g)} + H_2O_{(l)} + e^- \tag{10}$$

We know that acidic electrolyzer possesses large output current, but to date developed efficient OER catalysts in acidic solution are Ru/Ir oxides or alloys. Carbon-based materials are a group of materials that show promising application if the performance could be further boosted. Other materials suffer severe oxidation and corrosion under long time operation.

Although there is a general reaction path in adsorbates evolution mechanism, when considering different structural features in specific materials, new mechanisms like lattice O participated mechanism are proposed. Involving concrete catalyst, the participation of lattice O may occur on

Yaoyao Li is currently persuing her master degree under the supervision of Prof. Chengtao Yang at the University of Electronic Science and Technology of China (UESTC). Her research focuses on the design and synthesis of materials for electrocatalysis and energy storage.

Xinchuan Du is a senior student and will be a Ph.D. student under the supervision of Prof. Yanrong Li at UESTC. His research focuses on the design and synthesis of functional materials for energy storage and catalysis.

Jie Xiong is a full professor at UESTC. He received his Ph.D. degree in materials physics and chemistry from UESTC in 2007 and then performed postdoctoral research at Los Alamos National Laboratory from 2009 to 2011. His research interests focus on the synthesis structure–property mechanism of functional nanomaterials and energy materials and their applications.

different steps. For example, Xu's group suggests a lattice oxygen oxidation mechanism for direct O–O coupling on $Zn_{0.2}Co_{0.8}OOH$ catalyst.[9] Compared to catalytic mechanism, active center is another key point needing identification. From the perspective of thermodynamic stability, oxide or hydroxide is the most stable state under aqueous solution. To TM-Xides, the irreversible surface oxidation and structure transformation generates the metal oxyhydroxide. To perovskite oxides, the surface O vacancy plays as the active center with negligible structure change related to the low structure flexibility. Additionally, to evaluate the activity of catalysts using a uniform and regular index, some descriptors are concluded based on the empirical formulas, such as d-band center, e_g filling degree, and adsorption energy. In some cases, when adjacent atoms jointly contribute to the multistep catalytic process, adsorption energy could be regarded as a more proper activity descriptor for the whole reaction.

ADVANCED
SCIENCE NEWS
www.advancedsciencenews.com

NANO · MICRO
small
www.small-journal.com

2.2. Evaluation

Normal evaluation method toward OER includes the following parameters: overpotential (η), Tafel slope (b), stability, Faradic efficiency, and turnover frequency (TOF). Multi-criteria could lead to an equitable evaluation on OER performance.

The actual applied potential (E) in electrolysis is higher than E^0 in order to overcome kinetic energy barrier of catalyst. Overpotential (η) is the difference value between E and E^0 expressed in Equation (11). The reported η_{10} in most works is the overpotential value to reach a current density (j) of 10 mA cm^{-2}. Theoretical calculation formula (Equation (12)) derived from Nernst equation further explains the relation between E and E^0 (at 298.15 K and 1 atm situation). In the equation, n is the electron-transfer number of redox reaction, C_O and C_R are the concentrations of oxidized and reduced ions respectively

$$\eta = E - E^0 \tag{11}$$

$$E = E^0 + \left(\frac{0.0592}{n}\right) \lg \frac{C_O}{C_R} \tag{12}$$

$$\eta = a + b \lg j \tag{13}$$

The correspondence between logarithmic j and linear η can be depicted in a Tafel plot, and the linear part of it can further be fitted to Equation (13), where b refers to Tafel slope. Tafel slope indicates OER reaction rate, i.e., the increasing rate of j under the same potential rise.

Stability is an important indicator of OER performance. It could be demonstrated by time-dependent current (I–t) or potential measurement and cyclic voltammetry (CV) measurement for a long-time electrolysis.

Faradic efficiency refers to the desired charge utilization rate of catalyst. For OER, it can be expressed by the ratio of detected oxygen amount to the delivered total charges under a time-dependent potential or current measurement.

Turnover frequency is the efficiency of every active site per unit time. Accurate calculation of TOF is difficult to realize because accessible catalytic sites are just a portion of total materials. Effective method to obtain the precise number of surface reacting sites has been sought by many groups. TOFs based on total catalytic species still have reference values among similar materials.

Standardized measurement criteria have been established to provide a fair evaluation of OER performance. In a three-electrode system, corresponding linear sweep voltammetry (LSV), CV, chronoamperometry (CA), and chronopotentiometry (CP) measurements are performed to analyze the electrochemical performance of OER catalysts. However, the typical electrochemical curves usually undergo high anodic potential or large current density. As a result, the structure transformation-related signals are hidden. It is hard to distinguish difference and identify internal changes from rough measurements. According to these discussions, it is necessary to apply operando measurements to track the fleet changing of structure and potential intermediate state.

2.3. Surface Reconstruction

Larger coverage range of applied OER potential than the redox potential range of catalysts is the main reason for surface oxidation. Variable catalytic conditions, such like pH, temperature, and pressure, could modulate specific redox potentials and kinetics hence leading to multiple oxide products. It was suggested that high pH could facilitate reconstruction.[7a] Considering this fact and easy dissolution of TM-Xides in acid electrolyte, we mainly focus on the discussion in basic medium if not specially mentioned. And respective types of electrolyte, oxide product, and active species of TM-Xides discussed in following sections are tabulated and listed in **Table 1**.

Besides the changes from external OER conditions, structure variations of materials themselves would also induce differences in oxide products; especially the local structure changes like defects play a non-negligible role in reconstruction. This can still be attributed to the modulation of oxidation kinetics.

Catalytic reaction happens at the interface of catalyst surface and electrolyte, being significantly influenced by surface states. The specific role of surface reconstruction observed in recent years further implies the necessity of in situ analyses on materials and modulations of surface structure aiming at improving OER performance and confirming the real catalytic active site. Catalyst experiencing surface reconstruction in this review is called precatalyst.

Due to the harsh catalytic condition of OER, it is a great challenge for OER catalysts to maintain complete structure integrity after electrolysis. Taking noble-metal catalysts as an example, surface oxidation and dissolution of noble metal–based catalysts were noticed early in last century.[10] Dissolution of noble metals is a restrictive focus, with worse anticorrosion than their corresponding oxides and faster dissolution rate in base than in acid. And oxidation level of noble metal–based materials depends on applied potential range. Dissolution rates rank as following: Ru > Ir > RuO$_2$ > IrO$_2$, independent of the electrolyte.[11] Selective dissolution realized by alloying could lead to a better stability by sacrificing Ru on the surface of Ru$_{0.5}$Ir$_{0.5}$ alloy.[12] Formation of Ir^V was suggested to facilitate the deprotonation of OOH and subsequent oxygen formation.[13] High valence state noble metal ions are unstable to exist for a long time during OER. Unstable Ru^{VIII} and Ir^{VI} would form on Ir$_x$Ru$_{1-x}$O$_2$ surface both in acid and base, which then dissolved or regenerated to lower state ions quickly.[14] RuO$_4$ probably formed on the surface and dissolved quickly at a high potential above 1.45 V versus reversible hydrogen electrode (RHE).[15]

To reduce the high cost of catalyst from noble metal, non-noble metal catalysts are developed. Monometallic nanomaterials or multi-metal alloys are prepared as one family of OER catalysts. An oxide layer could easily form on the surface of TMs in alkaline solution. The main valence states of active metal ions on surface during OER will vary with different metal elements. Taking most common Ni, Co and Fe as examples, main existed states are Ni^{III}, Co^{IV}, and Fe^{IV}, respectively.[16] Reaction steps of metallic Co and Ni with the rise of potential are expressed as Equations (14)–(23) (Fe has a similar oxidaion process to Co). CoO$_2$ is unstable and will reverse to Co$_3$O$_4$ without applied high potential.[17] β-NiOOH phase will irreversibly convert into γ-NiOOH phase with a higher average valence state via overcharging.[18]

Table 1. The respective type of substrate, electrolyte, oxide product, active species, and reference of catalysts discussed in this review.
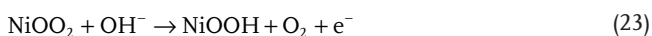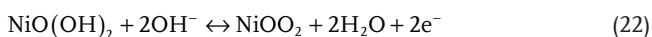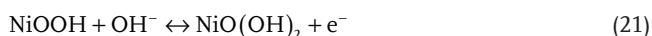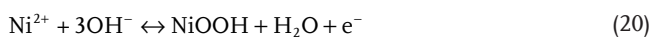
Catalyst	Substrate	Electrolyte	Oxide product	Active species	Ref.
Chalcogenide					
NiS	Ni Foam	1.0 M KOH	NiOOH	NiOOH@NiS	[27]
Ni_3S_2	Ni Foam	0.1 M KOH	Hydrated Ni oxide	$Ni^{0/1+/2+}$/hydrated Ni oxide	[26]
$Ni_xCo_{3-x}S_4/Ni_3S_2$	Ni Foam	1.0 M KOH	Ni–Co (oxy)hydroxide	Ni–Co (oxy)hydroxide	[28]
NiCoS	$Ti_3C_2T_x$	1.0 M KOH	NiCoOOH	NiCoOOH	[29]
MoS_2/Ni_3S_2	Ni Foam	1.0 M KOH	NiO	NiO/MoS_2	[22c]
CoS_x	$GCE^{a)}$	1.0 M KOH	CoOOH	CoOOH	[23]
$Co_{1-x}Ni_xS_2$	$NGA^{b)}$	1.0 M KOH	Co–Ni (hydro)oxide	Co–Ni (hydro)oxide/$Co_{1-x}Ni_xS_2$	[38]
NiSe	Ni foam	1.0 M KOH	$NiOOH, SeO_x$	NiOOH	[31]
NiSe	Ni foam	1.0 M KOH	NiO	NiO@NiSe	[36]
Fe–NiSe	FeNi foam	1.0 M KOH	$Ni(Fe)OOH, SeO_x$	Ni(Fe)OOH	[32]
$(Ni_{0.75}Fe_{0.25})Se_2$	$CFC^{c)}$	1.0 M KOH	$Ni_{1-x}Fe_xOOH$	$Ni_{1-x}Fe_xOOH$	[34]
$(Ni, Co)_{0.85}Se$	CFC	1.0 M KOH	γ-NiOOH	γ-NiOOH	[35]
$NiSe_2, CoSe_2$	GCE	1.0 M KOH	NiOOH, CoOOH	NiOOH, CoOOH	[37]
Pnictide					
CoP/C	GCE	0.1 M KOH	Co-oxy/hydroxide, PO_4^{3-}	Co-oxy/hydroxide	[45]
Ni_2P	GCE	1.0 M KOH	NiO_x	NiO_x	[47]
$Ni_2P_4O_{12}$	CFC	1.0 M KOH	Ni oxy/hydroxide	Ni oxy/hydroxide, $Ni_2P_4O_{12}$	[41c]
Ni_5P_4, Ni_2P	GCE	1.0 M KOH	Ni hydr/oxide, phosphate	Ni hydr/oxide	[46]
Ni–P	None	1.0 M KOH	$NiO/Ni(OH)_x$	$NiO/Ni(OH)_x$	[48]
FeP/Ni_2P	Ni foam	1.0 M KOH	Ni/Fe oxyhydr/oxide	Ni/Fe oxyhydr/oxide	[4e]
FeCoNiP	$CNF^{d)}$	1.0 M KOH	(Oxy)hydroxide	(Oxy)hydroxide	[55]
CoN	Ni foam	1.0 M KOH	Co_3O_4	Co_3O_4	[49]
Co_4N	CFC	1.0 M KOH	CoO_x	CoO_x	[40a]
$Co_{2/3/4}N$	GCE	0.1/1 M KOH	CoOOH	$CoOOH/Co_{2/3/4}N$	[50]
Ni_3N	GCE	1.0 M KOH	NiOOH	$NiOOH/Ni_3N$	[57]
Mn_3N_2	$FTO^{e)}$, Ni foam	1.0 M KOH	MnO_x	MnO_x	[51]
Carbide					
Mo_2C	$CS^{h)}$	1.0 M KOH	Mo oxide	Mo_2C	[59]
Mo_2C	Ni foam	1.0 M KOH	Mo oxide	Mo oxide	[60b]
$Ni–Mo_xC$	$NC^{i)}$	1.0 M KOH	NiOOH, Mo oxide	NiOOH	[61]
$Co–Mo_2C$	GCE	0.1 M KOH	CoOOH	CoOOH	[62]
Co_3C	GCE	1.0 M NaOH	CoO_x	CoO_x	[40b]
Boride					
Co_2B	GCE	0.1 M KOH	CoOOH	CoOOH	[65]
FeB_2	GCE	1.0 M KOH	FeOOH	FeOOH	[67]
$Co_{1/2/3}B$	$CFP^{j)}$, GCE	0.1/1 M KOH	Co_3O_4, CoOOH, B oxide	CoOOH	[68]
NiFeB	GCE	1.0 M KOH	γ-NiOOH, β-FeOOH	γ-NiOOH, β-FeOOH	[69]
$Ni–B_i$	FTO	1.0 M $KB_i^{f)}$	Ni^{4+} (γ-NiOOH like)	Ni^{4+} (γ-NiOOH like)	[70c]
$Ni–B_i$	Au Film	0.1 M KB_i	$Ni^{3.6+}$	$Ni^{3.6+}$	[71]
LiCoBPO, NaCoBPO	FTO, Ni foam	1.0 M KOH	$Co(OH)_2/CoOOH/CoO_x$	$Co(OH)_2/CoOOH/CoO_x$	[73]
Oxide/Hydroxide					
α-$Ni(OH)_2$	GCE	0.1 M KOH	γ-NiOOH	γ-NiOOH	[74a]
β-$Ni(OH)_2$	GCE	1.0 M KOH	β-NiOOH	β-NiOOH	[74b]
α-$Ni(OH)_2$	GCE	1.0 M KOH	γ-NiOOH	γ-NiOOH	[75]
NiFe–OH–F	Ni foam	1.0 M KOH	$NiFeO_x$	$NiFeO_x$	[76]

ADVANCED
SCIENCE NEWS
www.advancedsciencenews.com

NANO · MICRO
small
www.small-journal.com

Table 1. Continued.

Catalyst	Substrate	Electrolyte	Oxide product	Active species	Ref.
$NiCoO_xH_y$	FTO	0.1 M KOH	$NiOOH–h–CoO_2$	$NiOOH–h–CoO_2$	[77]
sAu/NiFe LDH	Ti mesh	1.0 M KOH	NiOOH	NiOOH	[78]
Tannin–NiFe LDH	CFP	1.0 M KOH	$Ni_xFe_{1–x}O_yH_z$	$Ni_xFe_{1–x}O_yH_z$	[79]
Co_3O_4	Au	0.1 M KOH	Co^{4+}	Co^{4+}	[81]
Co_3O_4	GCE	0.1 M $KP_i^{g)}$	$CoO_x(OH)_y$	$CoO_x(OH)_y$	[82a]
Ni–Co oxide	FTO	1.0 M NaOH	NiOOH	NiOOH	[83]
$ZnCo_{1.2}Ni_{0.8}O_4$	GCE	1.0 M KOH	NiOOH	NiOOH	[84]
BSCF82	GCE	0.1 M KOH	Co_3O_4-like	Co_3O_4-like	[85]
BSCF	GCE	0.1 M KOH	CoO(OH), FeO(OH)	CoO(OH), FeO(OH)	[86]

a)Glassy carbon electrode; b)Nitrogen-doped reduced graphene oxide aerogel; c)Carbon fiber cloth; d)Carbon nanofiber; e)Fluorine tin oxide; f)Borate; g)Phosphate; h)Carbon sheet; i)N-doped graphene/carbon nanotube hybrid; j)Carbon fiber paper.

For metal–organic complexes, tunable coordination environment and structure make them potential materials for OER. Designing specific structure of metal–organic complexes could help investigate the mechanism for OER. The unstability resulted from easy dissociation of organic ligands during electrocatalysis could expose inner active metal species or facilitate oxy/hydroxide formation. For example, tannic acid in tannin–NiFe complex film could leach out from the surface and expose the inner $Ni_xFe_{1–x}O_yH_z$ active sites to improve activity.[19] The precursor role of metal organic complex to form active hydroxide was suggested to be more important than stability during OER, i.e., functioning as a platform for real active sites' formation[20]

$$Co + OH^- \rightarrow CoOH + e^- \tag{14}$$

$$CoOH + OH^- \rightarrow Co(OH)_2 + e^- \tag{15}$$

$$Co(OH)_2 + OH^- \rightarrow CoOOH + H_2O + e^- \tag{16}$$

$$3Co(OH)_2 + 2OH^- \rightarrow Co_3O_4 + 4H_2O + 2e^- \tag{17}$$

$$Co_3O_4 + H_2O + OH^- \rightarrow 3CoOOH + e^- \tag{18}$$

$$CoOOH + OH^- \rightarrow CoO_2 + H_2O + e^- \tag{19}$$

$$Ni^{2+} + 3OH^- \leftrightarrow NiOOH + H_2O + e^- \tag{20}$$

$$NiOOH + OH^- \leftrightarrow NiO(OH)_2 + e^- \tag{21}$$

$$NiO(OH)_2 + 2OH^- \leftrightarrow NiOO_2 + 2H_2O + 2e^- \tag{22}$$

$$NiOO_2 + OH^- \rightarrow NiOOH + O_2 + e^- \tag{23}$$
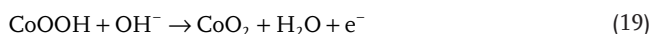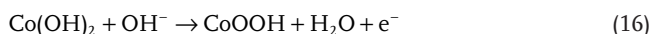
Considering the multi-type of TM-Xides, we will detailedly discuss the structure evolution of TM-Xides in the following sections. Here, it could be concluded that the evolution phenomenon is tending to achieve a same result with oxide or (oxy)hydroxide covering the external surface. This is revealed by various characterization methods, like TEM, XPS, and Raman. Such results exhibit well agreement with the thermodynamic rules.

3. Group VIA X: Chalcogenide

TM-Xides, where X from group IIIA to VIA are classified here for detailed discussions. The structure, performance, and activity mechanism are investigated and concluded for rational evaluations toward OER electrocatalysts. In this section, 2D chalcogenides are firstly emphasized due to their special structure and electronic properties.

Chalcogenide is an important group of electrocatalyst family for water splitting.[21] The most reported metal chalcogenides with remarkable catalytic performance for OER are the cobalt-based or nickel-based chalcogenide materials. Interestingly, a number of groups have noticed the surface oxidation of metal chalcogenide catalysts during OER via surface analysis techniques such as XPS, TEM, and Raman spectrum,[22] especially the in situ analysis applications directly observing the evolution of morphology and structure during OER process to identify the real active sites.[23] Additionally, theoretical calculations are performed to investigate the specific atomic configurations to discuss the possible reaction mechanism according to the experimental results. Furthermore, by comparing the performances of multi-metal chalcogenides to that of monometallic chalcogenides, it is found that bimetallic or multi-metal chalcogenides show better activity, indicating the important role of metallic synergistic effect for OER.[24]

3.1. Structure Transformation

Usually, X-ray diffraction (XRD) is a simple and valid method to distinguish crystal structure of materials. However, due to the very thin and low-crystallinity of formed oxy/hydroxide layer on catalyst surface, it could be difficult to be detected by XRD.[25] We could only observe a clear decline of diffraction peaks and speculate the possible decomposition. Thus diverse analysis techniques are developed to demonstrate the structure change.

ADVANCED
SCIENCE NEWS
www.advancedsciencenews.com

NANO · MICRO
small
www.small-journal.com

For example, the formation of nickel oxide species on the surface of Ni_3S_2 grown on Ni foam (Ni_3S_2/Ni) was revealed via post-OER scanning electrochemical microscopy (SEM) and XPS analyses.[26] After CV measurement, the high-resolution XPS peak of Ni_3S_2 at 852.7 eV disappeared with a decreasing intensity ratio of primary peaks (855.2, 872.7 eV) to satellite peaks (860, 879 eV) simultaneously, which meant the appearance of high valence oxide species, while it was not detected in the XRD results. The similar phenomenon was also noticed by Zhu et al. in their work about NiS microsphere film.[27] After 20 h stability test at 290 mV, the thin NiOOH layer on the surface of NiS was further confirmed by Raman spectra. Besides obtaining evidence from the spectroscopy method, micrology methods like SEM and TEM directly provide visual features of structural evolution. Wu et al. noticed the total conversion of monodispersed $Ni_xCo_{3-x}S_4$ nanoparticles into amorphous oxy/hydroxide layer (underlying Ni_3S_2 partially preserved) in TEM, after a robust OER stability test for 30 h at $\eta = 160$ mV under $I-t$ mode.[28] Disappearance of Ni/Co−S bonds and positive shifts of Ni/Co 2p peaks in XPS proved the oxidation of NiCoS/$Ti_3C_2T_x$ [T_x is −(F_x) or −$(OH)_x$ surface terminal group] (**Figure 1**a).[29] The morphology transformation from nanosheets into nanoparticles of NiCoS exhibited absolute structural reconstruction. The in situ formed thin NiO layer with a lattice distance of 0.21 nm and a thickness of 12.6 nm on Ni_3S_2 surface were revealed by TEM investigations.[22c] On the other hand, high crystallinity oxyhydroxide species could be detected via XRD. The diffraction peaks of crystallized CoOOH oxidized from amorphous CoS_x could be clearly observed in XRD, which was also revealed by selected area electron diffraction (SAED) patterns.[23] Especially, a pseudo-in situ TEM and energy dispersed X-ray spectroscopy (EDS) analysis showed a clear surface evolution of CoS_x in alkaline solution via anodization at 10 nA for different times. When the time increased from 0 to 12.5 min, oxygen became enriched on surface, along with the reduction of cobalt or sulfide concentration (Figure 1b–d). Step-by-step phase evolution was further illustrated by CP test at 0.5 mA cm^{-2} without any pre-activation process or treatment (Figure 1e). CoS_x firstly converted into $Co(OH)_2$ intermediate (<0.6 h), then $Co(OH)_2$ converted into CoOOH and accomplished until ≈1.1 h. Inconsistent with the stable curve in CP test at 10 mA cm^{-2}, potential measured at 0.5 mA cm^{-2} was rising until 1.1 h. Researchers suggested that pre-activation treatment or high applied current density could accelerate CoOOH formation, sequentially resulting in an unawareness of intermediate formation during OER. OER stability performance in literatures may need to be reconsidered based on this phenomenon. As it is aforementioned, a robust performance of catalyst during OER stability test does not mean that structure integrity is maintained before and after the OER process.
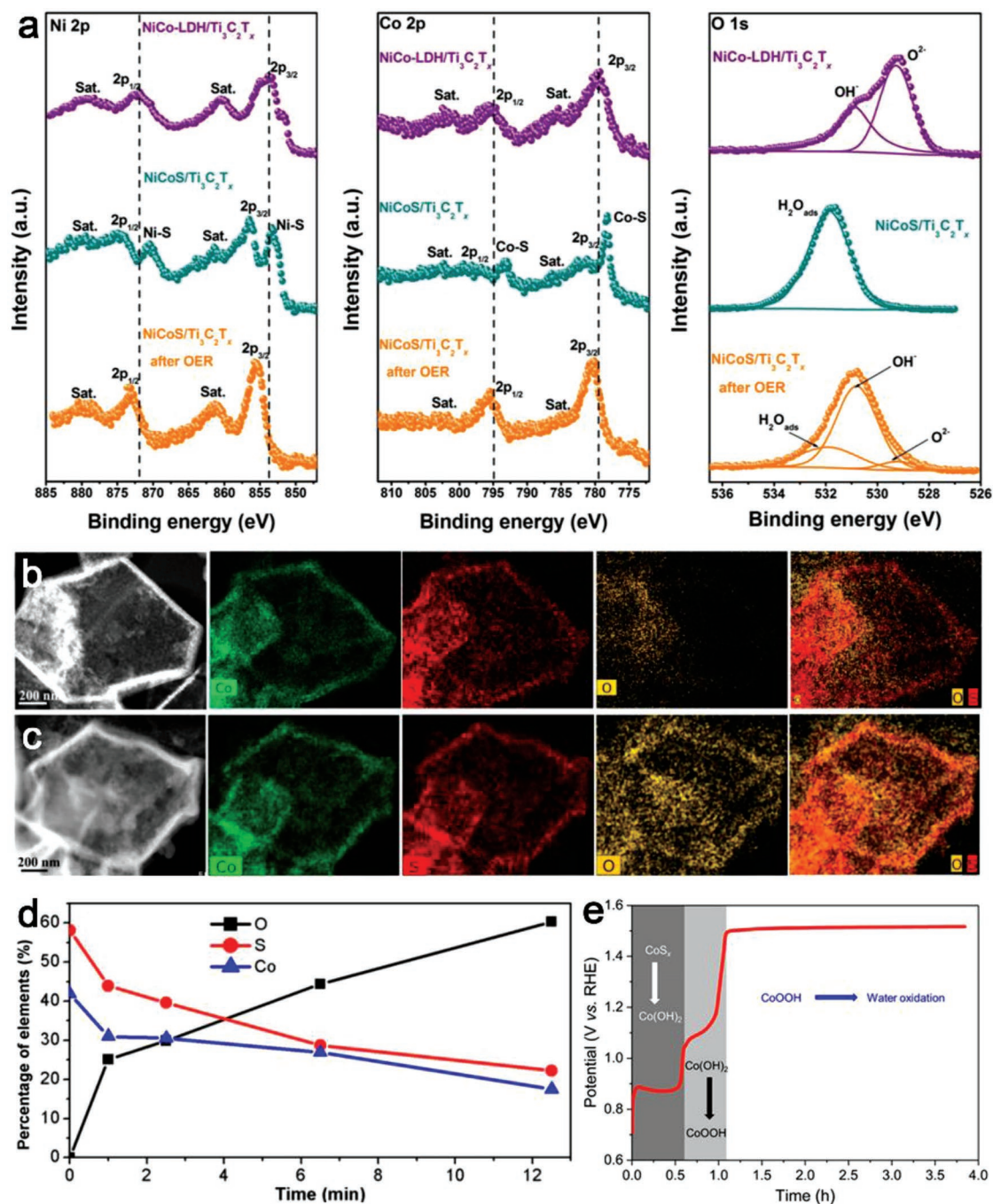
To selenide, surface phase transition not only includes oxy/hydroxide formation, but also contains conversion to selenium oxide.[30] By comparing the XPS signals of Se on NiSe nanowires from the air-exposed sample before OER and the post-OER product, a stronger oxidation peak of SeO_x was detected after OER electrocatalysis, consistent with the increased peak intensity of Ni oxides.[31] Inductively coupled plasma mass spectrometry (ICP-MS) measurements showed a degradation of Se during OER operating for 24 h at 500 mA cm^{-2}, with a final disappearance of it and an enrichment of SeO_x in XPS spectra.[32]

In addition, it is worth noting that the crystallinity of in situ formed oxy/hydroxides on catalyst surface is different among various works. In many cases, it is amorphous.[28,33] The formation mechanism of that still needs further studies. The formed Ni(Fe)OOH skin on Fe-doped NiSe nanoflake arrays was confirmed to be amorphous.[32] Similarly, $Ni_{1-x}Fe_xOOH$ formed on $(Ni_{0.75}Fe_{0.25})Se_2$ nanosheets had a low crystallinity based on the broad peak in post-XRD.[34] Nevertheless, in some cases, it possesses crystalline structure. Xia et al. found that the NiOOH covering the $(Ni, Co)_{0.85}Se$ nanotube arrays was γ phase.[35] Additionally, NiO also tended to form during catalysis in Ni-based materials.[36,22c] Here, we also highlight that the degree of oxidation transformation reaction highly depends on operation time under high oxidizing potential. It was reported that the proceeding time of surface Co/NiOOH formation started at the onset value of OER.[37] While the oxidation of Ni-doped CoS_2 integrated on N-doped reduced graphene oxide aerogel (CNS–NGA) was suggested to begin until long-term test.[38] These may be related to the anti-oxidation ability of different materials. In the meanwhile, from the thermodynamic perspective, it can be concluded that the ending state of most OER catalysts is the oxide within sufficient time.

3.2. Mechanism

Gradually, the formed metal oxy/hydroxide is identified as the main active species for high OER catalytic activity, while the roles of other parts of catalysts lack enough attentions for the performance.[39] For example, there is no rational explanation for the influence of increased content of formation of SeO_x on the surface. Some works noticed that the external oxy/hydroxide layer reached a relatively steady state during proceeding OER stability test.[40] It is suggested that the formed oxide shell could protect inner structure against the further oxidation. It may be possible that the formed SeO_x could be adsorbed on the edge or layer of hydroxide. Thus a few SeO_x could exist and be detected. The coexistence of these oxide species may contribute to the electronic transfer or surface hydrophilicity under long-term stability, which possibly deserves further research.

As quantities of works suggested, the synergetic effect between surface oxy/hydroxide and the inner unoxidized material is crucial to OER performance. Due to the in situ formation process, the strongly coupled interface between upper oxy/hydroxide and inner chalcogenide facilitates the charge transfer from active sites to conductive substrates. Notably, good conductivity greatly contributes to high OER performance. In order to make this theory more persuasive, the activity comparison between metal chalcogenide and metal oxy/hydroxide catalysts was performed. When Ni–Co oxide and hydroxide catalysts were prepared alone, the surface oxidation reaction did not achieve such better activity, because the underneath sulfide/selenide was conductive and could improve the electron accessibility of surface active sites.[28] From this standpoint, engineering of special structures like core–shell framework or interface combining outside oxy/hydroxide layer and inner chalcogenide core were also synthesized by some groups as an efficient way to enhance OER activity. The in situ formed NiO/MoS_2 from pristine MoS_2/Ni_3S_2 heterostructure was favorable

**ADVANCED
SCIENCE NEWS**

www.advancedsciencenews.com

NANO · MICRO

small

www.small-journal.com

Figure 1. a) XPS spectra of Ni 2p, Co 2p, and O 1s of NiCo–LDH/Ti$_3$C$_2$T$_x$, NiCoS/Ti$_3$C$_2$T$_x$, and post-OER NiCoS/Ti$_3$C$_2$T$_x$. Reproduced with permission.[29] Copyright 2018, American Chemical Society. HAADF images and EDS mappings of CoS$_x$ b) before OER and c) after OER for 12.5 min. d) O, S, and Co proportion variation on time during OER. e) CP curve of CoS$_x$ at 0.5 mA cm^{-2}. Reproduced with permission.[23] Copyright 2018, American Chemical Society.

for OER catalysis.[22c] Density functional theory (DFT) calculations were further performed to investigate the adsorption free energies of H and OH intermediates. MoS$_2$ could easily chemisorb H, while NiO or Ni$_3$S$_2$ could easily chemisorb OH. This led to decreased energy barriers for water dissociation and faster conversion of reaction intermediates. Thus the structure effect improved the OER activity (**Figure 2**a). The synergetic effect was also supported by other DFT calculations of multistep

reaction energy barriers and charge distribution analyses. Four-electron OER steps corresponding to adsorptions of OH*, O*, OOH*, and O$_2$ (expressed in Equations (7)–(10), respectively) were spontaneous in Ni-doped CoS$_2$ integrated on N-doped reduced graphene oxide aerogel (CNS–NGA) except for step III (Equation (9)) (bias voltage was 1.23 V_{RHE}), and the main reaction sites changed compared with CNS.[38] Charge distribution region became larger in CNS–NGA, namely the delocalization
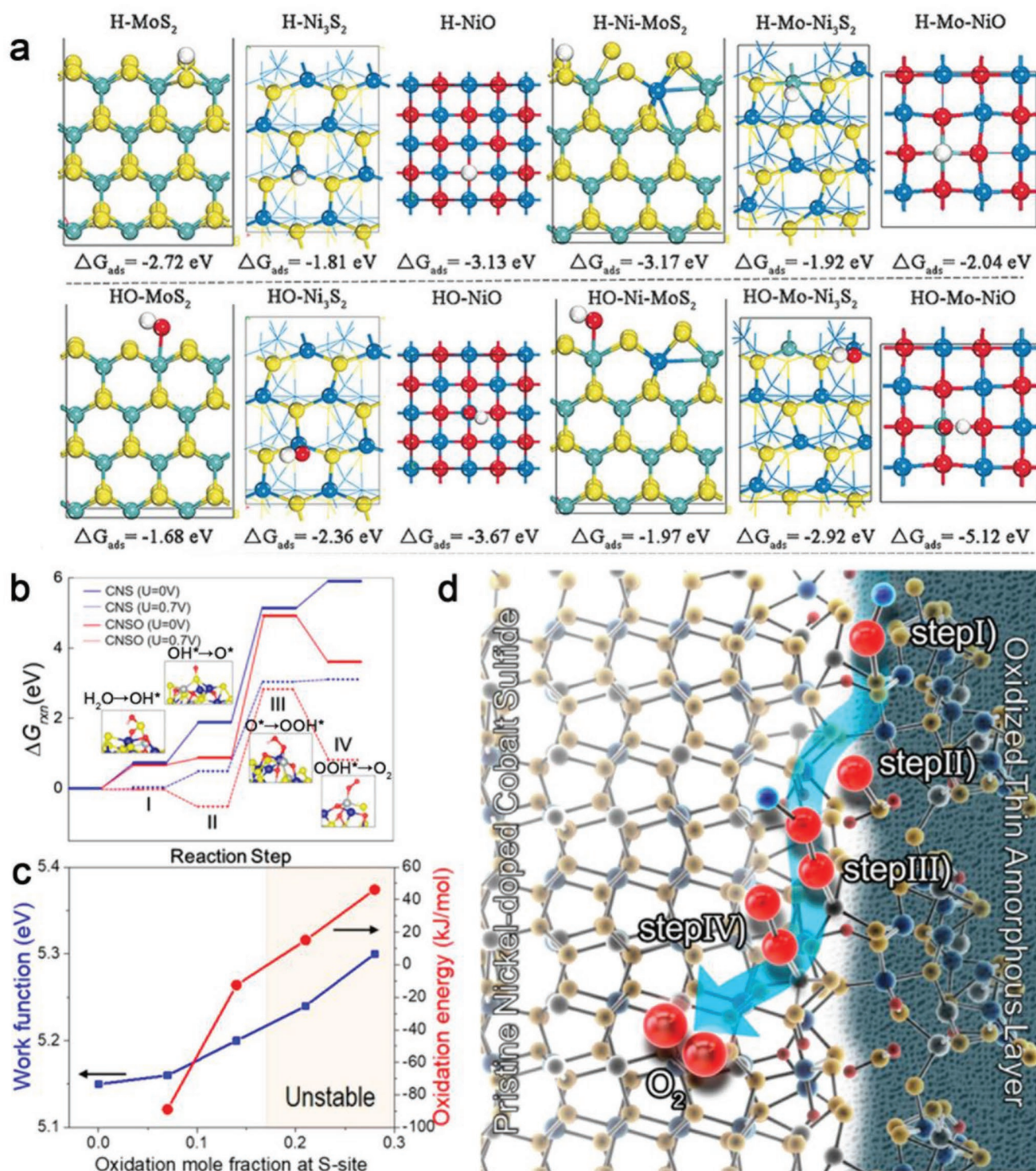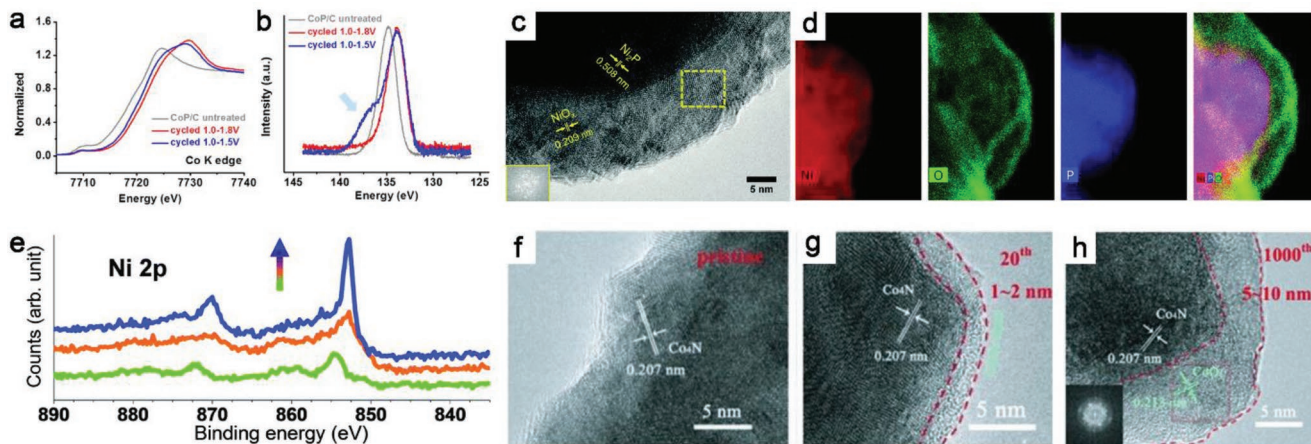
Figure 2. a) Chemisorption models and energies of H/OH intermediates on MoS_2, Ni_3S_2, NiO surfaces, or heterostructures coupled by them. Atoms in yellow, green, blue, white, and red represent S, Mo, Ni, H, and O, respectively. Reproduced with permission.[22c] Copyright 2016, Wiley-VCH Verlag GmbH & Co. KGaA, Weinheim. b) Calculated adsorption energy landscapes for CNS and CNSO with $U = 0/0.7$ V. Steps I, II, III, and IV correspond to formation of OH*, O*, OOH*, and O_2 respectively. c) Evolution of work function and oxidation energy of CNS versus oxidation mole ratio at S sites. d) OER pathways at CNS and CNSO borders. Reproduced with permission.[38] Copyright 2018, American Chemical Society.

through the whole catalyst. A strong hybridization between N 2p and Co 3d orbits existed according to density of states (DOS) plots, forming covalent bonds that promote charge transfer by reducing contact resistance. The respective role of Co, S, Ni, N atoms was illustrated. S atoms were the main reaction sites for steps I (Equation (7)) and II (Equation (8)) and could easily lose

ADVANCED
SCIENCE NEWS
www.advancedsciencenews.com

NANO · MICRO
small
www.small-journal.com

Figure 3. a) XANES and b) P 2p XPS of CoP nanoparticles after two cycles at 5 mV s^{-1}. Reproduced with permission.[45] Copyright 2015, American Chemical Society. c) HRTEM image of Ni$_2$P after electrolysis at 1.5 V versus RHE for 1 h, inset is FFT of the selected area. d) EDX mappings of Ni, O, and P corresponded to the region exhibited in (c). e) High-resolution depth-profiling XPS of Ni 2p. Reproduced with permission.[47] Copyright 2015, The Royal Society of Chemistry. HRTEM images of Co$_4$N after f) 0, g) 20, and h) 1000 CV cycles; inset is FFT of selected area. Reproduced with permission.[40a] Copyright 2015, Wiley-VCH.

an electron, facilitating OER. Ni atoms and Co atoms were the main sites for steps III and IV (Equation (10)), respectively. The energy barriers and DOS of oxidized catalyst (CNSO–NGA) were also calculated (Figure 2b,c). DOS indicated that surface oxidation had little impact on the metallic properties of CNS. The increased work function due to the increasing substitution ratio of O for S indicated a more obvious band bending of CNS–NGA interface, facilitating charge transfer. The calculated maximum substitution ratio of 17% for O:S maintained a stable oxidative surface structure. Additionally, according to DFT results, steps I and II became dominant on oxidized part of the catalyst, along with step III and IV happening primarily on unchanged part (Figure 2d). Thus, such structure evolution created a better reaction path for oxygenic intermediates with lower energy barriers. These tailored surface states boost the catalytic performance improvement and maintain the whole structure stability.

4. Group VA X: Pnictide

Similar to metal chalcogenide, a thin oxy/hydroxide layer could also easily form on the surface of metal nitride and phosphide during OER catalytic process.[41] Since metal nitride and phosphide are quite sensitive to air, consequently, they are locally oxidized before OER in some cases,[42] leading to a more complex surface structure for OER.[43] Usually, considering the similar evoluted structure after OER, the slight natural oxidation is ignored. To visualize the formation process of oxy/hydroxide layer, several research groups characterized this phenomenon by diverse approaches, focusing on the proceeding time, elemental content variation, and morphology change during OER at varying stages.[44]

4.1. Structure Transformation

For phosphide, dephosphorization was commonly observed during OER in some reports, accompanying with surface

oxidation. A detailed morphology and component analyses of cobalt phosphide nanoparticles were provided by Ryu et al.[45] The nanotopography exhibited a conspicuous change from original rod-shaped CoP into porous nanoweb architectures in the first CV cycle. The decline of P:Co ratio detected by EDS indicated the separation and solution of part of P species. Emphatically, in the first scan a huge oxidation peak was obtained before the onset potential of OER (≈1.5 V), thus the observed morphology transition might proceed during oxidation process prior to OER. The subsequent ex situ X-ray absorption near edge structure (XANES), extended X-ray absorption fine structure (EXAFS) and XPS were employed to investigate the chemical states of the activated species. It was demonstrated that both Co and P experienced state changes. A positive edge energy shift about ≈5 eV in XANES convinced the oxidation of Co (**Figure 3**a), and a binding energy shift of P in XPS showed the transformation of original metaphosphate P–O species (PO$_3^-$) into phosphate groups (PO$_4^{3-}$) (Figure 3b), which agreed well with the declination of P:Co ratio. EXAFS spectra further confirmed that Co-oxo/hydroxide clusters loosely dispersed in a phosphate-enriched amorphous network. Apart from Co-based materials, investigations of nickel phosphide (Ni$_2$P, Ni$_5$P$_4$ complex) before and after OER measurement (1.5 V vs RHE for 1 h) also showed remarkable surface change.[46] Nickel oxy/hydroxide nanoparticles on the surface of original nanoplates were confirmed by XPS and TEM analyses. The XPS peak intensity increase of oxidized Ni species and the increment of O:P atomic ratios (from about 3.1:1 to 14.3:1) were revealed after OER. Hu's group also observed the surface oxide layer of post-OER Ni$_2$P.[47] After the transformation from Ni$_2$P to NiO$_x$ during pre-activating process, the oxide layer seemed to become stable in latter oxygen evolution reaction. An obvious core–shell structure combined surface oxide layer and inner Ni$_2$P particle was observed in high resolution TEM (HRTEM) and EDS mapping (Figure 3c,d). High-resolution depth-profiling XPS was used to analyze the Ni 2p, P 2p, and O 1s regions. For Ni, with the increase of profiling depth, the full width at half maximum decreased and Ni content increased (Figure 3e). Similarly, the

ADVANCED
SCIENCE NEWS
www.advancedsciencenews.com

NANO · MICRO
small
www.small-journal.com

decline of P content and increment of O content were observed, jointly illustrating that the metallic Ni_2P core was coated by an oxide layer. Wang et al. reported a time-varying surface oxidation of nickel phosphide during OER.[48] They adopted a long-term OER durability measurement of the porous Ni_5P_4–NiP_2/Ni_2P (Ni–P) foam, and analyzed the surface morphology, structure and composition evolutions at different electrolytic time via SEM, EDS, and TEM. After 20 min, the sheet-shaped morphology was well maintained but the surface became rough. Comparing the XPS results of post-OER Ni–P foam with that of the untreated one, a new strong oxygen peak appeared, indicating the formation of oxygen species on the surface. TEM analysis revealed that poor crystalline NiO was the main composition of surface oxide layer. When the electrolysis time prolonged to 60 and 180 min, the sheet structure became fractured and coarser. 600 min later, the geometric structure of Ni-based electrode had changed dramatically and only Ni and O were detected by EDS. The obvious structure investigations suggest most pnictide as good precatalysts for OER. The evolved structure plays the key role in catalytic reaction.

Nitride has a similar surface evolution as phosphide in the catalytic process of OER. The thickness of CoO_x formed on surface of Co_4N porous nanowires increased and became stable (5–10 nm) with the rise of CV cycles, based on HRTEM analyses (Figure 3f–h).[40a] Fourier transformed extended XAFS (FT-EXAFS) characterization for Co_4N before and after 1000 potential cycles at 0–0.8 V (vs Ag/AgCl) confirmed surface oxidation. After 1000 cycles, FT peak intensity of Co—Co bond (at 2.5 Å) showed a significant decrease, and the length of Co—Co was between that of standard Co foil and Co_3O_4. Furthermore, the weaker edge at ≈7712 eV in XANES after cycling suggested a dealloying process. Similar oxidation of CoN was observed and a 5–10 nm thick Co_3O_4 layer was detected by TEM after a long durability test (10, 30, and 50 mA cm^{-2} in sequence) over 30 h with a small overpotential variation.[49] Other cobalt nitrides in different stoichiometric ratios (Co_2N, Co_3N, and Co_4N) were all demonstrated with the in situ formed CoO_2 layers after electrocatalytic process.[50] An amorphous MnO_x shell formed on Mn_3N_2 crystal surface after long-term electrolysis was detected by TEM.[51] In the following XPS results, the binding energy difference between Mn $2p_{1/2}$ and its satellite raised from original 10.8 to 11.8 eV, suggesting the ion pair conversion from Mn^{2+}/Mn^{3+} to Mn^{3+}/Mn^{4+}.

As one derivative from Group VA P element, the structure of phosphates is relatively more stable than phosphide. In most cases, phosphate is used as catalyst in neutral solution with slight structural change. However, characterizations suggested that phosphate experienced structure transformation during OER under alkaline media.[52] The relatively higher content of Ni and O compared with P (Ni:P:O ratio varied from 0.6:1:3.97 to 2.12:1:16) after OER revealed surface corrosion and reconstruction of $Ni_2P_4O_{12}$ (NPO) nanocrystals.[41c] Surface distorted amorphous structure about 1 nm thickness was also observed in Xu and co-workers' work.[53]
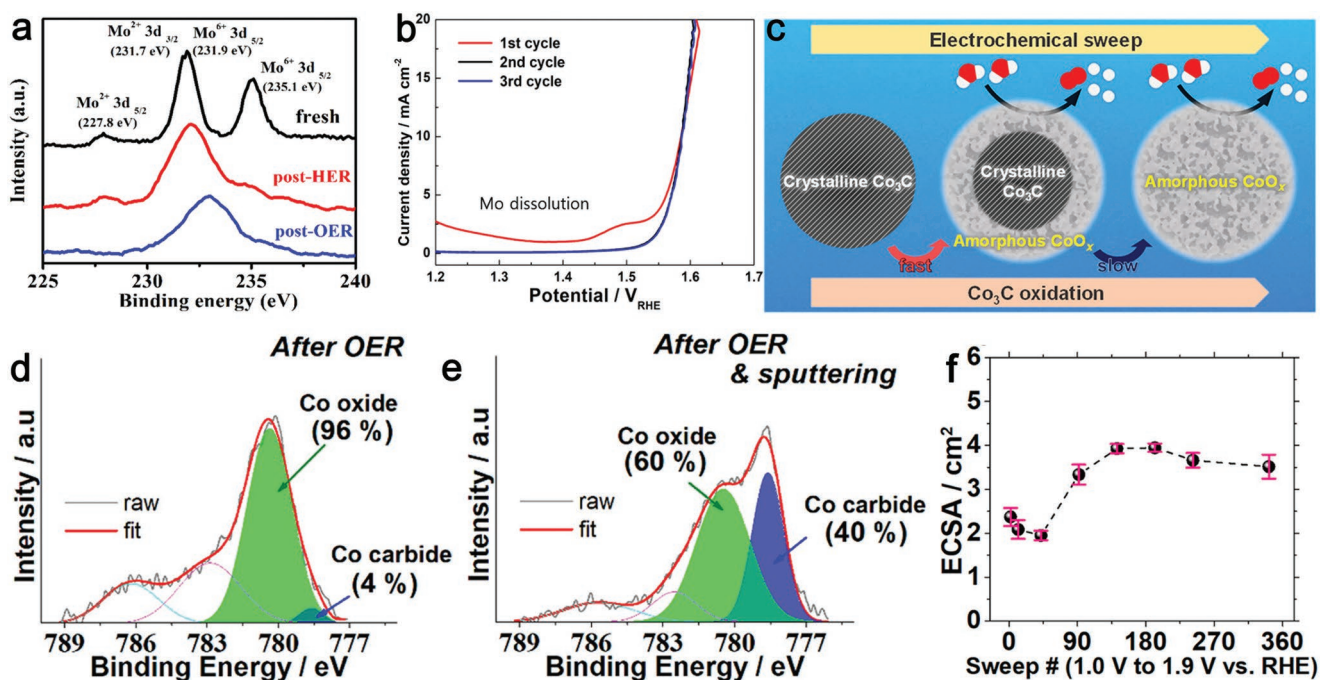
4.2. Mechanism

More and more works try to confirm that the metal nitride and phosphide are precatalysts acting as conductive support and the catalytic sites are on the in situ formed shell. The catalytic

reaction mechanism on this active shell has become a focus in the field of water splitting.[54]

Yu et al. reported that oxides formed on surface of FeP/Ni_2P hybrid could facilitate proton-coupled electron transfer process during OER, enhancing activity along with interface effect between two different phosphides.[4e] Additionally, the secondary or trinary metal introduction was demonstrated beneficial to enhance OER activity. Thus a series of TM phosphides were synthesized regarded as precatalysts. Among them, FeCoNiP was found out to be the most active OER catalyst. It was identified that the introduction of heterogeneous metal atoms facilitated local electron transfer between metal and P, leading to an enhanced oxidizing state of metal centers.[55] As a result, the metal synergy boosts the activity improvement.[56] It has also been a valid modification strategy.

The catalytic mechanism of oxy/hydroxide shell of Ni_3N in alkaline electrolyte was the similar as other Ni-based materials in previous section.[18,57] The first three steps were relatively slow and reversible which determined the OER rate, while step 4 was faster than previous steps and irreversible. At about 1.4 V versus RHE, original Ni^{2+} could be oxidized into Ni^{3+} and formed NiOOH/Ni_3N intermediate state. With the increase of anodic potential, surface NiOOH could be firstly oxidized into $NiOO_2$ and then regenerated to NiOOH due to O_2 release. The underneath Ni_3N served as an excellent conductive substrate which could dramatically decrease the electron conduction barrier between surface active sites and electrode. When comparing the performance of NiOOH/Ni_3N with as-prepared NiO nanosheet, NiOOH/Ni_3N exhibited more effective electronic supplement and more intense oxidation peak which suggested that the in situ formed active sites were more active than NiO nanosheet with the same specific surface areas. These structure reconstructions ultimately enhanced the catalytic efficiency. As reported by Xie's group, CoOOH firstly formed on the surface of initial Co_4N porous nanowires, and then oxidized into CoO_2 at a higher potential, forming a more active complex structure with Co_4N during OER.[40a] Moreover, it was suggested that CoO_x could protect the inner Co_4N from further oxidation besides providing active sites, based on the increasing activity during first 20 cycles and then stablizing in following cycles. This suggestion might provide a possible explanation for the coexistence of surface transformation and good electrochemical stability.

Distinct from phosphide, flexible structures with diverse orientations of phosphate groups could improve stability of phosphates by changing their local coordination state of metal center. To clearly find out the catalytic species in neutral solution, Bard's group investigated CoP_i catalysts by surface interrogation SEM.[58] By applying this surface-selective measurement in special solvents, they could directly detect the density of active sites that water could easily access on CoP_i surface. This in situ and direct detection could exactly calculate the turnover frequency of the catalytic site and lead to a clear understanding of catalytic mechanism. By titrating separately $Co^{III/II}$ and $Co^{IV/III}$ redox couple at the surface, the rate constants of Co^{III} and Co^{IV} in the reactions with H_2O were 0.19 and >2 s^{-1}, respectively by time-dependent measurements. A fast reaction kinetics of Co^{III} with water suggested that Co^{III} generated from Co^{II} possibly played an important role in OER. In basic solution, our group also revealed the formation of oxy/hydroxides and suggested a

**ADVANCED
SCIENCE NEWS**

www.advancedsciencenews.com

NANO · MICRO

small

www.small-journal.com

Figure 4. a) XPS spectra of Mo 3d for original, post-OER and post-HER Ni–Mo$_x$C/NC. Reproduced with permission.[61] Copyright 2018, American Chemical Society. b) Current density curves versus potential (vs RHE) after first, second, and third OER cycle of Co–Mo$_2$C. Reproduced with permission.[62] Copyright 2018, Elsevier B.V. c) Schematic oxidized process of Co$_3$C particles. Post-XPS spectra of Co 2p$_{3/2}$ region for d) Co$_3$C and e) Co$_3$C with Ar+ sputtering. f) Variation of ECSA with raised sweep number of Co$_3$C particles. Reproduced with permission.[40b] Copyright 2018, American Chemical Society.

positive effect of them on OER performance. A better activity after stability test indicated by polarization curve of NPO/CC (CC represents carbon cloth) was ascribed to synergetic effect between NPO and oxy/hydroxide.[41c] In addition, surface amorphization increased the active sites of crystalline structure and changed the surface adsorptivity state.

5. Group IVA X: Carbide

Compared with metal compounds mentioned above, surface oxidation phenomenon of metal carbide was not investigated sufficiently. The oxidation of molybdenum carbide or its complex structure such as M/Mo$_x$C (M refers to Co or Ni nanoparticles) shows a similar structure reconstruction compared to aforesaid pnictide. Differently, on one hand, Ni or Co could easily form NiOOH or CoOOH phase on catalyst surface during OER process. On the other hand, it was considered that the oxidation of molybdenum carbide could also facilitate the activity enhancement. But the relation between molybdenum oxide and Co/Ni oxyhydroxide was not clearly studied. Although the oxidation of other metal carbides as OER catalysts shows the same functional mechanism as pnictide, further researches still need to be adopted in order to understand the specific effect of multi-oxide.

5.1. Structure Transformation

Carbide is identified as efficient electrocatalysts for water splitting. However, it also suffers the problem of clear identification of real active site for OER, even though the electrochemical stability is excellent. An obvious example is that an ignorable current loss is observed during long time stability test, but the post-OER characterization shows obvious surface oxidation of Mo$_2$C after 1000 CV cycles.[59] It is confusing that the detailed investigation toward the surface oxidation is not performed. Some work observed oxidation of carbide but did not discuss specific mechanism. According to Raman spectroscopy, small quantity of MoO$_3$ was detected on Mo$_2$C surface, even though the ratio of MoO$_3$/Mo$_2$C was variational during an OER cycle.[60a] The higher percentage of Mo^{4+} (229.8 and 233.8 eV) and Mo^{6+} (232.6 and 235.7 eV) in post-XPS spectra determined the formation of Mo oxides.[60b] To Ni/Mo$_x$C (MoC, Mo$_2$C) nanoparticles on N-doped graphene/carbon nanotube (Ni-Mo$_x$C/NC), Ni was considered as the main reason for NiOOH formation on the surface.[61] Meanwhile, Mo$_x$C was also oxidized during OER, supported by a positive binding energy shift of Mo 3d in post-OER electrode (**Figure 4**a). Besides, obvious energy shift of Co 2p and higher ratio of oxo species of Co–Mo$_2$C than Co nanoparticles after only three cycles indicated a fast surface oxidation.[62] Dissolution of Mo was also mentioned in this work. The conversion of most of Mo$_2$C into MoO$_4^{2-}$ was mainly observed during the first cycle in Figure 4b due to its instability in OER conditions and special structure effect. For single Mo$_2$C, Mo oxide was detected on the surface of post-OER catalyst; however, the existence of MoO$_4^{2-}$ ion in solution was not measured in most researches. In another example, a complete conversion from Co$_3$C particles into amorphous CoO$_x$ particles was observed and the role of CoO$_x$ in OER were reported by Kim et al. detailedly (Figure 4c).[40b] After 2 LSV sweeps, a ≈4 nm

ADVANCED
SCIENCE NEWS
www.advancedsciencenews.com

NANO · MICRO
small
www.small-journal.com

amorphous layer formed on the surface in HRTEM image. Then XPS analysis of this post-LSV catalyst after Ar^+ sputtering treatment indicated a higher proportion of carbide (40%) than the untreated one (4%) (Figure 4d,e), which further supported the existence of core–shell structure. The estimated electrochemically active surface area (ECSA) was increasing with raised LSV sweeps and became stable after ≈150 sweeps. It was believed that after 150 sweeps, Co_3C had been totally oxidized into CoO_x (supported by SAED and XRD results) (Figure 4f). The larger ECSA normalized current densities of in situ formed CoO_x compared to that of commercial CoO particles strongly demonstrated the intrinsic high activity of formed CoO_x.

5.2. Mechanism

It was suggested that synergetic effect between carbide and in situ formed oxide species is vital in OER activity, while strong evidence needs to be further provided. Cui's group suggested a positive influence from the oxidation of Mo on OER activity for MoO_2.[63] It was presumed that the oxidation facilitated the performance improvement of Ni/Mo_xC.[61] Additionally, by comparing the oxidation peaks (≈1.36 V vs RHE) in polarization curves of catalysts with different Mo contents, the coupling between Ni and Mo_xC was believed to be beneficial for NiOOH formation. Negative binding energy shift of Mo 3d in XPS compared with Mo_2C indicated the electron transfer between Ni and Mo_xC, confirming their viewpoint. To Co/Mo_2C heterostructure, the interface of Mo_2C and Co nanoparticles facilitated the formation of CoOOH and electron transfer, leading to an overpotential decrease of 30 mV at 10 mA cm^{-2} compared with that of single Co nanoparticles.[62] The calculated DOS indicated an energy upshift about ≈0.25 eV of Co d-band center in regard to Femi level, which improved the adsorption capacity toward OH^-. Although the role of CoOOH has been analyzed, the possible influence from the Mo oxide is not efficiently demonstrated. Promising progress is still needed in order to clarify the relation between diverse metal oxide species. What is more, to pure Co/Ni carbide, Kim et al. suggested that Co_3C was just a precatalyst and the in situ formed CoO_x was the real active species (Figure 4c).[40b] To make it clear, researchers normalized the current density by ECSA and discovered that CoO_x had a higher intrinsic activity (380 mV at 0.1 mA cm^{-2}) than commercial CoO (430 mV at 0.1 mA cm^{-2}) particles. The increasing ECSA during OER (before ≈150 LSV sweeps) indicated that formed CoO_x was the main reason for activity enhancement. After 150 sweeps, the totally transformed structure from Co_3C to CoO_x gradually exhibited a relatively stable performance, which meant that the CoO_x played as the real contributor for the catalytic performance during proceeding operation more than 150 sweeps.

6. Group IIIA X: Boride

There are just a few researches of metal boride electrocatalysts for OER compared to metal chalcogenide and pnictide. However, in situ oxidized species could still be characterized.[64] The interaction between B and metal atom could strengthen M—B or B—B bonds and weaken M—M bonds. As a result, the induced covalent character and lattice strain further decreased the energy barrier of OOH* formation and improved the OER activity.[65] Based on above analysis, modulating the B content could provide an effective way to enhance catalytic properties.[66]

Similar to aforementioned sections, the surface of metal boride undergoes oxidation to form oxy/hydroxide in OER process. A series of species conversions of these oxidation resultants might happen with the catalytic reaction proceeding. The main species formed on FeB_2 surface was α-Fe_2O_3 after 1 h OER.[67] But it totally converted into amorphous FeOOH after further 12 h long test (**Figure 5**a,b). By comparing the activity of FeB_2 with hydrothermal synthesized FeOOH and Fe_2O_3, it was demonstrated that the FeB_2 sample exhibited better performance and the inner FeB_2 core facilitated electron transfer for enhanced OER activity. Besides, the firstly observed CoO/$Co(OH)_2$ on Co_xB (x = 1, 2, 3) surface further transformed into Co_3O_4/CoOOH under the increased anodic potential.[68] Co_3O_4 might facilitate the oxidation from Co^{2+} to Co^{3+}, hence it led an easier $CoOOH/CoO_2$ formation. As reported, the surface B in all Co_xB samples was converted into B oxides, based on the enlarged B oxide peak and disappearance of B 2p peak in XPS spectra. It was noteworthy that negligible current degradation was observed at 50 mA cm^{-2} for 12 h. This seemed to suggest that Co_2B was a rather robust electrocatalyst. However, the post-OER characterizations showed apparent surface polycrystalline CoOOH (Figure 5c,d). Such results demonstrated that the evolution signal of geometric structure was covered under the superior electrochemical stability. To Ni-based boride, besides the formation of γ-NiOOH layer (Figure 5e), B concentration was also detected in electrolyte.[69] It is known that B could be oxidized into borate ion which could easily diffuse into the solution. The quantitative experiments showed that about 28.8–32.9% B was detected in electrolyte within 45 min CV cycles using inductively coupled plasma optical emission spectroscopy measurements (Figure 5f). In addition, borate (B_i) in electrolyte was believed to enhance the proton-coupled electron transfer process,[70] hence facilitating the OER performance of NiFeB nanoparticles. The obtained common conclusion is that the active species is the surface reconstructed metal oxyhydroxide.

In addition, as one derived group, borate is also efficient catalyst for OER that would undergo surface oxidation in some cases. Anodization of Ni–B_i thin films in 1.0 M KB_i solution led to a rise of average oxidation state of Ni ions from +3.16 to +3.6 and a structure conversion from bis-oxo/hydroxo bridged Ni into edge-sharing NiO_6 octahedra, revealed by XANES and EXAFS respectively.[70c] Based on this discovery, the edge of NiO_6 was considered as OER site supported by in situ O K-edge XAFS datas.[71] When the applied potential increasing to 0.6 V, the peak intensity of NiO_6 octahedra began to rise, and then reached a stable state after 0.8 V. Moreover, no obvious reduction of NiO_6 to Ni^{2+} was detected when potential decreased from 0.9 to 0.5 V. Thus it indicated that the activity came from the edge of NiO_6. Borophosphate could combine the advantages of borate and phosphate, or even has distinct characteristics compared with them. Variable anionic groups link with others in diverse ways, thus creating rich structure chemistry.[72] A 420 nm thick CoO_x shell was observed on the surface of helical borophosphate $LiCo(H_2O)_2[BP_2O_8]\cdot H_2O$ (LiCoBPO) after
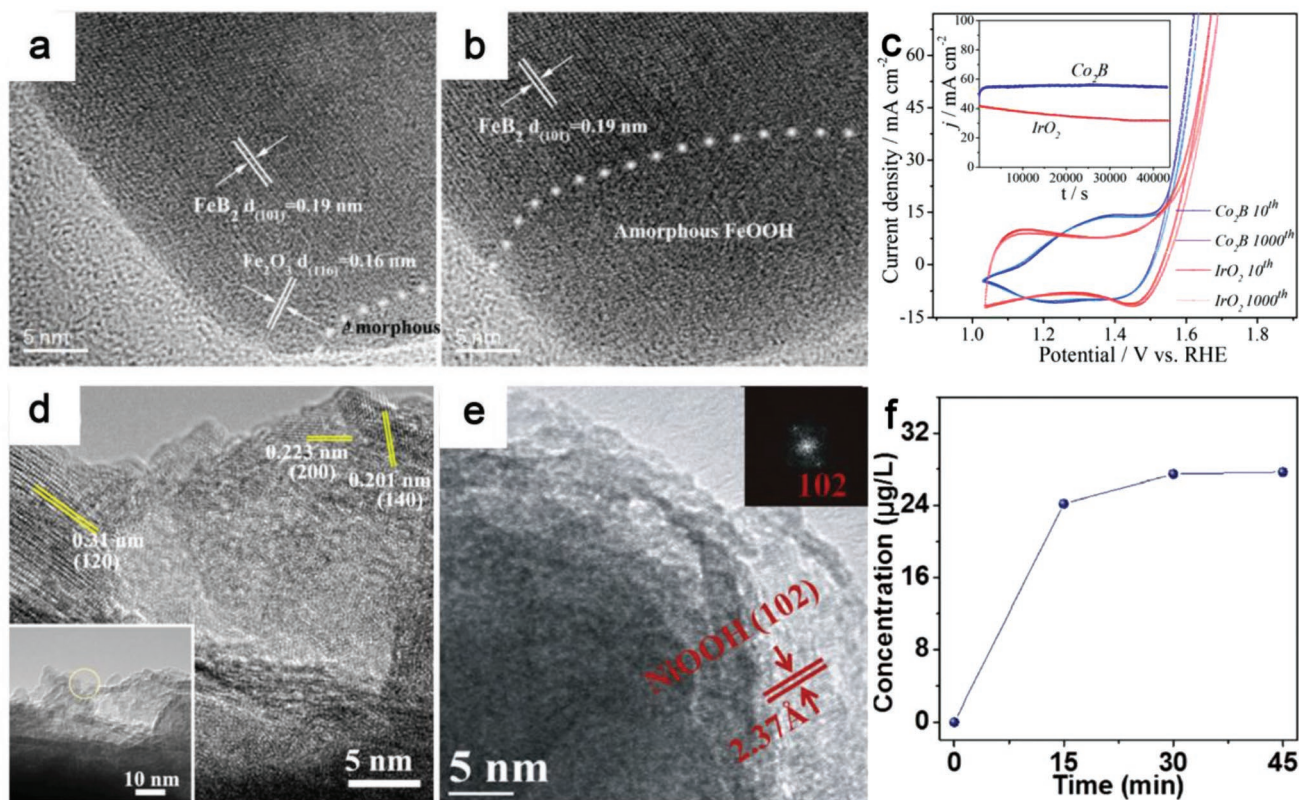
Figure 5. a) TEM images of FeB$_2$ after OER for 1 h and b) 12 h. Reproduced with permission.[67] Copyright 2017, Wiley-VCH. c) CV curves after 10 and 1000 cycles of Co$_2$B and IrO$_2$; the inset are time-dependent current density curves for the two catalysts at 345 mV. d) HRTEM images of Co$_2$B after durability test at 50 mA cm^{-2} for 12 h; inset is the corresponding TEM image. Reproduced with permission.[68] Copyright 2017, American Chemical Society. e) HRTEM images and f) ICP–OES results of B concentration variation during CV (20 mV s^{-1}, 1.0–1.8 V vs RHE) of NiFeB nanoparticles; inset of (e) is corresponding FFT. Reproduced with permission.[69] Copyright 2017, Tsinghua University Press and Springer Nature.

stability measurement,[73] also demonstrated by the decreased distance between Co 2p$_{1/2}$ and Co 2p$_{3/2}$ signals (from 16 to 15.1 eV). It was believed contributing to the OER activity.

7. Others: Hydroxide and Oxide

Apart from aforesaid typical chalcogenide, pnictide, carbide, and boride, surface reconstruction also happens in hydroxide catalysts. The reconstructed surface state with new phase dramatically boosts the OER performance. Taking Ni(OH)$_2$-based materials as examples, during the OER, the surface of Ni(OH)$_2$-based materials could dynamically reconstruct oxy(hydroxide) layers.[74] The converted active phase is identified as the true reactive sites. So the faster formation of active phase, the stable and better performance could be achieved. To decrease the formation energy of γ-NiOOH and accelerate the phase formation, nickel vacancies (V_{Ni}) were introduced into initial α-Ni(OH)$_2$.[75] The calculated formation energies showed a reduced tendency from 2.50 to 1.96 eV with V_{Ni} concentrations increasing from 0% to 11.1% (**Figure 6**a).

Interestingly, in some cases, anion hybrid hydroxides could generate new surface structure distinct from direct-transformed NiOOH phase. For example, the CV cycling method was employed by Hu's group to treat the F-doped NiFe hydroxide

(NiFe–OH–F).[76] Unexpectedly the OER activity of postcycling NiFe–OH–F at η = 220 mV increased over 58-fold along with a decreased Tafel slope. Through detailed SEM and TEM investigations, they clearly observed the surface amorphization of crystalline NiFe–OH–F on the postcycling sample (Figure 6b,c). F proportion reduced from 15.5 to 0.57 at% under EDX spectra (Figure 6d). In comparison with the postcycling results of NiFe–OH electrode without F, fluoride element leaching induced the formation of mesoporous and amorphous NiFe oxide during the electrochemical process, which contributed to the activity improvement. Koel's group employed thermal and electrochemical adjustment process to pretreat CoO$_x$H$_y$ and NiCoO$_x$H$_y$ catalyst films.[77] By virtue of operando Raman spectroscopy and electrochemical measurements, they observed the reversible structural evolutions of NiCoO$_x$H$_y$ and electrochemical pretreated CoO$_x$H$_y$ samples during the electrocatalytic process (Figure 6e,f). The identification of the characteristic peaks indicated that the NiOOH–h–CoO$_2$ structure could be the real catalytically active phase of NiCoO$_x$H$_y$ materials for oxygen evolution. NiOOH formation on single Au atom supported on NiFe layer double hydroxide (sAu/NiFe LDH) was revealed by in situ Raman. A charge modulation on active Fe caused by sAu could facilitate adsorption of reactants hence improving activity.[78] The modulation of local structure rather than the bulk Ni(Fe)O$_x$H$_y$ provided a potential strategy on enhancing OER activity.[79]
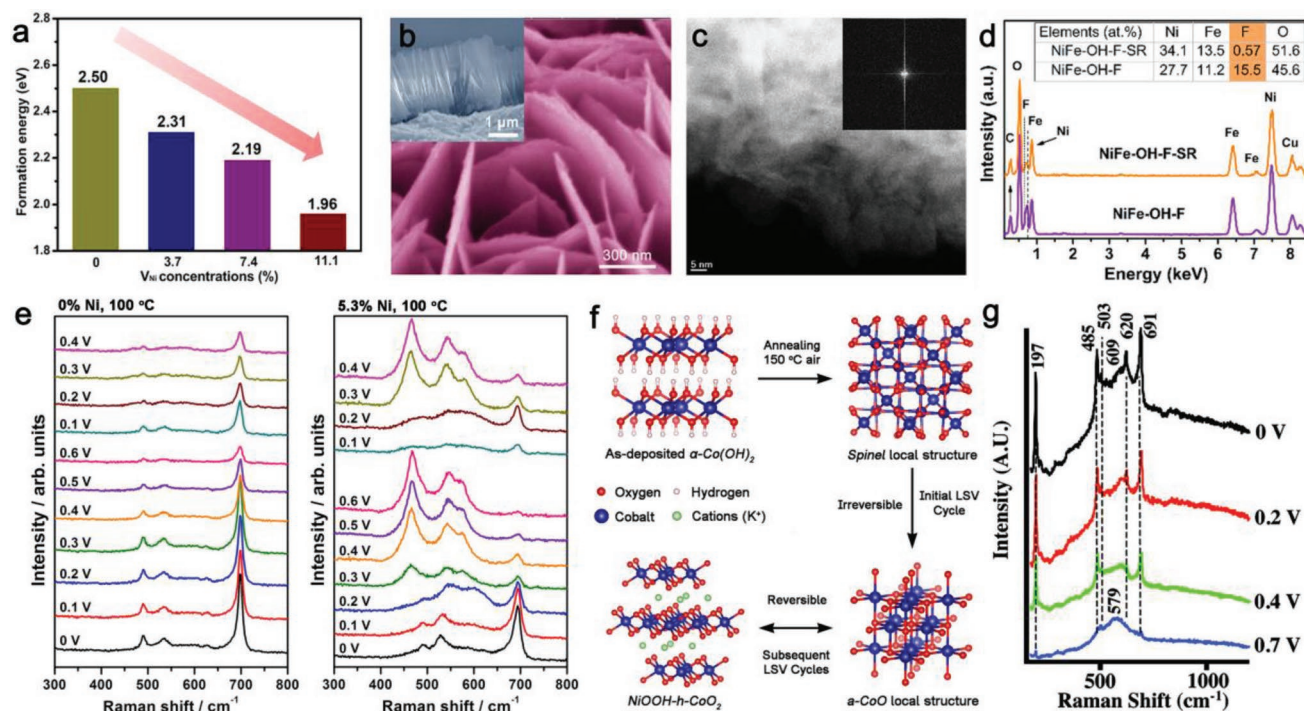
Figure 6. a) γ-NiOOH formation energies with different V_{Ni} concentrations. Reproduced with permission.[75] Copyright 2018, American Chemical Society. b) SEM and c) high-resolution, high-angle annular dark-field scanning transmission electron microscopy (HAADF–STEM) images of surface reconstructed NiFe–OH–F (NiFe–OH–F–SR). Insets are the lateral views of NiFe–OH–F–SR layer and FFT image, respectively. d) EDX spectra of NiFe–OH–F and NiFe–OH–F–SR. Reproduced with permission.[76] Copyright 2018, American Chemical Society. e) Raman spectra of Co-100 and $Ni_{5.3}$Co-100 catalyst at various potentials versus Ag/AgCl (samples were annealed at 150 °C in air for 1 h followed behind the furnace preheated to 100 °C, denoted as these formulas). f) Schematic graph of the conversion of $Ni_{5.3}$Co-100 during OER. Reproduced with permission.[77] Copyright 2017, American Chemical Society. g) Operando Raman spectra of ≈87 ML (monolayer equivalents) cobalt oxide/Au. Reproduced with permission.[81] Copyright 2011, American Chemical Society.

On the other hand, the surface structural conversion also occurs on oxides during electrochemical process at high anodic potential. Activation treatment was early applied to improve activity.[80] However, convincing and comprehensive mechanism studies were not enough until in situ methods were developed. Yeo and Bell performed operando surface-enhanced Raman spectroscopy to investigate the surface oxidation of Co_3O_4.[81] They found the formation of Co^{IV} species under high OER potential condition by comparing and analyzing the evolution of Raman peaks at 579 cm^{-1} (Figure 6g). The 4+ oxidation state is believed as the active center during O_2 evolution. Another important evidence for the change of surface structural features of Co oxide was observed by Strasser and Chen groups using in situ X-ray spectroscopy.[82] The transformed CoOOH from Co_3O_4 or exterior atomic-layer CoO played as the real active species toward OER in neutral condition.[82b] They further confirmed that the surface pre-reduced CoO layer could act as an effective buffer layer to inhibit the structural destruction to Co_3O_4 scaffold from induced strain during phase transformation.

In some cases, two typical oxides, spinel (AB_2O_4) and perovskite (ABO_3) oxides, also underwent surface reconstruction. Specially, selective oxidation and dissolution of A or B site ions induced active composition segregation provide a potential strategy to tailor OER activity. K-edge energy shift of Ni from 8350.2 to 8350.7 eV in in situ XANES when applying 2.0 V_{RHE} indicated the formation of NiOOH, which acted as

active sites.[83] No clear shift of Co with same applied potential compared with open circuit suggested the coordination and conductor role. The formation of active NiOOH and leaching of Zn and Co in metastable $ZnCo_{1.2}Ni_{0.8}O_4$ were also confirmed by HRTEM and scanning transmission electron microscopy energy-dispersive X-ray spectroscopy (STEM-EDS).[84] Diminishing peaks at 532 eV in K-edge electron energy loss spectroscopy (EELS) of O further indicated the increasing O vacancies and structure relaxation during OER.

$Ba_{0.5}Sr_{0.5}Co_{0.8}Fe_{0.8}O_{3-\delta}$ (BSCF82) experienced surface amorphization and formed an ≈10 nm thick spinel-Co_3O_4-like layer during OER revealed by HRTEM and Raman spectroscopy, along with the leaching of A-site cations (Ba^{2+} and Sr^{2+}).[85] Higher potential (above 1.5 V_{RHE}) led to a thicker amorphous layer and hence improving OER activity. Specially, surface reconstruction of $Ba_{0.5}Sr_{0.5}Co_{0.8}Fe_{0.2}O_{3-\delta}$ (BSCF) with a slight dissolution was suggested to enhance OER activity.[86] In other word, lower energy barrier for reconstruction of catalyst during OER could be the key point for high performance. Until the potential reached 1.425 V_{RHE} (equal to OER onset potential), a positive energy shift of Co K-edge under in situ XAS appeared, becoming higher with the subsequent potential rise to 1.55 V_{RHE}. Descend of the potential from 1.55 to 1.2 V did not lead to a reversed shift of Co, indicating an irreversible oxidation. Higher intensity at 2.6 and 3 Å in FT-EXAFS spectra further suggested CoO(OH) and FeO(OH) formation

**ADVANCED
SCIENCE NEWS**
www.advancedsciencenews.com

**NANO · MICRO
small**
www.small-journal.com

respectively, accompanied by the dissolution of Ba and Sr observed in XAS. Similarly, leaching of Sr^{2+} of $SrCo_{0.95}P_{0.05}O_{3-\delta}$ (SCP) led to the formation of a deficient protective layer and a larger exposure of surface area.[87] Subsequently it facilitated the partial oxidation of Co^{3+} into Co^{4+} which served as active sites together with surface vacancies. Incorporation of Fe in $La_{0.2}Sr_{0.8}Co_{1-x}Fe_xO_{3-\delta}$ enhanced surface oxy(hydroxide) formation without changing its oxidation state.[88]

Here, it is concluded that the dynamically formed oxyhydroxide is identified as a crucial intermediate during OER. In most cases, the critical phase transition during reconstruction is reversible during testing.[77,82] But this does not mean that the initial surface structure is completely maintained after oxygen catalysis. A special structure may reconstruct on the surface as the stable state like CoO. Such phenomenon is not observed in some other metal (hydro)oxides, involving the active role of O vacancies and B site ions in perovskite and spinel oxides.[89]

8. Conclusions and Outlook

Surface of catalyst is where the catalytic reaction occurs. It plays a crucial role for efficient electrocatalysis. To date, the structural evolution at high anodic potential has attracted enormous attentions in order to unravel the effective active sites for oxygen catalysis. Although progresses have been achieved with the development and application of in situ characterization techniques, there is still a long way to totally lift the veil of catalytic centers of various inorganic nanomaterials. To general sulfide, pnictide, carbide, boride, and part oxide/hydroxide, continuous researches gradually observe and identify the surface structural features during OER. It is sure that the derived amorphous/crystalline species from the inevitable oxidation procedure contribute to oxygen evolution with tuned energy barriers and conductivity. However, the surfaces in some reports are also observed maintaining the original states of the composites after catalysis. This may be the specific effect of interface structure and insufficient electrolysis time.

In this review, we highlight the critical role of electrochemical tuning surface on achieving a high catalytic efficiency. The self-converted structure not only exhibits better hydrophilicity but also accelerates water adsorption and dissociation. What is more, the reconstructed surface structure usually exhibits amorphous phase or defect-rich state, which possesses highly active catalytic sites with unsaturated metal atom coordination. On another hand, the self-doping effect occurring during the surface oxidation could change the electron density of states around the doping sites, which directly tunes the adsorptivity toward reaction intermediates. But it is always ignored due to some reasons like lack of exact detection. Additionally, conductivity also shows significant influence on catalytic performance. It is noteworthy that chalcogenide, phosphide, nitride, and carbide have metallic property in most cases. After surface reconstruction, the synergetic effect between external active layer and internal conductive supporter facilitates the multistep catalytic reactions via better charge transfer and distorted top crystal structure.

Surface reconstruction is an efficient way for TM-Xides to adapt to the harsh electrolytic environment and improve activity. It usually begins when the OER reaction starts and reaches a balance under long time electrolysis. But referring to certain material, the oxidative degree depends on the nature of the material. Thus oxidation accompanies with the stability. Here, it is worth noting that in most reported OER stability measurements, the post-OER samples exhibit external oxidation layer. In the meanwhile, the electrochemical stability shows very stable current or potential curves. As a result, it is concluded that reconstructed surface structure maintains or results in the stability. Different materials, local structures, and electrochemical conditions lead to changeable compositions of reconstruction products. Special structure designs of precatalysts like surface activation, interface engineering, defect fabrication and selective surface etching were adopted by some groups to reduce the energy barrier for reconstruction. Surface reconstruction regulation via structure design is a potential way to improve OER performance of TM-Xides.

As the role of oxidation and dissolution of by-products such as SeO_x and MoO_4^{2-} remains unclear on catalytic process, a lot of questions still exist, for example, whether the adsorption of these by-products on the surface could facilitate the reactions. Could the easier oxidation and dissolution of X element facilitate the formation of hydroxide? Whether there are different reconstruction phenomena in different electrolytes. To unravel these questions, more systematical works deserve to be done. Additionally, the reversibility of oxy/hydroxide formation in different cases also deserves further researches. Diverse behaviors of reconstruction even among congeneric materials still lack rational explanations at atomic scale. Systematic characterization methods and analytic theories are needed to be established in order to accelerate the understanding and development of oxygen catalysis.

Although various operando characterization methods have been adopted to investigate the catalytic features during reactions, the activity discription is still insufficient. Most characterizations base on single species identification, thus the difficulty on identification of real active structure at atomic level limits the deep understanding of catalytic process. For example, the in situ soft XAS analyses demonstrate the existence of Ni^{4+} species located at 875.1 eV when the applied potential rising to above 1.6 V, but it is also hard to identify the detailed states of surface structure, including the stress, crystalline degree and thickness, which directly relate to the catalytic activity.[90] Spectrum methods like Raman can identify the formed (oxy)hydroxide active species, but it could not recognize the adsorptivity of surface ligands. Considering the complex surface environment and reversibility of active species, combination of multi-technique to in situ characterize the OER process at nano scale can provide powerful evidences for understanding the catalytic mechanism.

Besides above discussions, we present the outlook on further studies aiming to pave the development of OER catalysts. First, a comprehensive understanding of reconstruction process should be gained by monitoring the evolution of reaction interface via in situ technique development, involving the influences from the reconstructed by-products and electrolyte. Second, theoretical analyses based on in situ characterizations should be consummated to help determine the activity origin of OER catalyst and specific correlation between local structure and reconstruction. Third, based on the mature characterizations

1901980 (15 of 18)

and systematical theories, in terms of thermodynamics, structural modulation or design of precatalyst will be an efficient strategy for facilitating surface reconstruction and hence achieving OER activity improvment.

Conflict of Interest

The authors declare no conflict of interest.

[1] a) V. R. Stamenkovic, D. Strmcnik, P. P. Lopes, N. M. Markovic, *Nat. Mater.* **2017**, *16*, 57; b) X. Zou, Y. Zhang, *Chem. Soc. Rev.* **2015**, *44*, 5148; c) Z. W. Seh, J. Kibsgaard, C. F. Dickens, I. Chorkendorff, J. K. Norskov, T. F. Jaramillo, *Science* **2017**, *355*, eaad4998; d) I. Roger, M. A. Shipman, M. D. Symes, *Nat. Rev. Chem.* **2017**, *1*, 0003.

[2] a) B. M. Hunter, H. B. Gray, A. M. Muller, *Chem. Rev.* **2016**, *116*, 14120; b) R. Subbaraman, D. Tripkovic, K. C. Chang, D. Strmcnik, A. P. Paulikas, P. Hirunsit, M. Chan, J. Greeley, V. Stamenkovic, N. M. Markovic, *Nat. Mater.* **2012**, *11*, 550; c) C. Spori, J. T. H. Kwan, A. Bonakdarpour, D. P. Wilkinson, P. Strasser, *Angew. Chem., Int. Ed.* **2017**, *56*, 5994; d) J. Huang, J. Gao, Y. Xia, Y. Sun, J. Xiong, Y. Li, S. Cong, J. Guo, S. Du, G. Zou, *Nano Energy* **2018**, *46*, 305.

[3] a) B. Zhang, X. Zheng, O. Voznyy, R. Comin, M. Bajdich, M. García-Melchor, L. Han, J. Xu, M. Liu, L. Zheng, F. P. G. d. Arquer, C. T. Dinh, F. Fan, M. Yuan, E. Yassitepe, N. Chen, T. Regier, P. Liu, Y. Li, P. D. Luna, A. Janmohamed, H. L. Xin, H. Yang, A. Vojvodic, E. H. Sargent, *Science* **2016**, *352*, 333; b) M.-I. Jamesh, X. Sun, *J. Power Sources* **2018**, *400*, 31; c) T. Zhang, Y. Zhu, J. Y. Lee, *J. Mater. Chem. A* **2018**, *6*, 8147; d) K. Fan, Y. Ji, H. Zou, J. Zhang, B. Zhu, H. Chen, Q. Daniel, Y. Luo, J. Yu, L. Sun, *Angew. Chem., Int. Ed.* **2017**, *56*, 3289; e) J. Huang, J. Chen, T. Yao, J. He, S. Jiang, Z. Sun, Q. Liu, W. Cheng, F. Hu, Y. Jiang, Z. Pan, S. Wei, *Angew. Chem., Int. Ed.* **2015**, *54*, 8722; f) J. Ping, Y. Wang, Q. Lu, B. Chen, J. Chen, Y. Huang, Q. Ma, C. Tan, J. Yang, X. Cao, Z. Wang, J. Wu, Y. Ying, H. Zhang, *Adv. Mater.* **2016**, *28*, 7640.

[4] a) P. Cai, J. Huang, J. Chen, Z. Wen, *Angew. Chem., Int. Ed.* **2017**, *56*, 4858; b) A. Dutta, A. K. Samantara, S. K. Dutta, B. K. Jena, N. Pradhan, *ACS Energy Lett.* **2016**, *1*, 169; c) Y. Yang, K. Zhang, H. Lin, X. Li, H. C. Chan, L. Yang, Q. Gao, *ACS Catal.* **2017**, *7*, 2357; d) Y. Liu, C. Xiao, M. Lyu, Y. Lin, W. Cai, P. Huang, W. Tong, Y. Zou,

Y. Xie, *Angew. Chem., Int. Ed.* **2015**, *54*, 11231; e) F. Yu, H. Zhou, Y. Huang, J. Sun, F. Qin, J. Bao, W. A. Goddard 3rd, S. Chen, Z. Ren, *Nat. Commun.* **2018**, *9*, 2551; f) L. Liu, H. Zhao, Y. Lei, *InfoMat* **2019**, *1*, 74.

[5] D. Yan, Y. Li, J. Huo, R. Chen, L. Dai, S. Wang, *Adv. Mater.* **2017**, *29*, 1606459.

[6] K. Zhu, X. Zhu, W. Yang, *Angew. Chem., Int. Ed.* **2019**, *58*, 1252.

[7] a) H. Jiang, Q. He, Y. Zhang, L. Song, *Acc. Chem. Res.* **2018**, *51*, 2968; b) N. T. Suen, S. F. Hung, Q. Quan, N. Zhang, Y. J. Xu, H. M. Chen, *Chem. Soc. Rev.* **2017**, *46*, 337.

[8] a) B. R. Wygant, K. Kawashima, C. B. Mullins, *ACS Energy Lett.* **2018**, *3*, 2956; b) S. Jin, *ACS Energy Lett.* **2017**, *2*, 1937.

[9] Z.-F. Huang, J. Song, Y. Du, S. Xi, S. Dou, J. M. V. Nsanzimana, C. Wang, Z. J. Xu, X. Wang, *Nat. Energy* **2019**, *4*, 329.

[10] R. Kötz, H. Neff, S. Stucki, *J. Electrochem. Soc.* **1984**, *131*, 72.

[11] S. Cherevko, S. Geiger, O. Kasian, N. Kulyk, J.-P. Grote, A. Savan, B. R. Shrestha, S. Merzlikin, B. Breitbach, A. Ludwig, K. J. J. Mayrhofer, *Catal. Today* **2016**, *262*, 170.

[12] N. Danilovic, R. Subbaraman, K. C. Chang, S. H. Chang, Y. Kang, J. Snyder, A. P. Paulikas, D. Strmcnik, Y. T. Kim, D. Myers, V. R. Stamenkovic, N. M. Markovic, *Angew. Chem., Int. Ed.* **2014**, *53*, 14016.

[13] H. G. Sanchez Casalongue, M. L. Ng, S. Kaya, D. Friebel, H. Ogasawara, A. Nilsson, *Angew. Chem., Int. Ed.* **2014**, *53*, 7169.

[14] M. E. Lyons, S. Floquet, *Phys. Chem. Chem. Phys.* **2011**, *13*, 5314.

[15] a) A. R. Zeradjanin, A. A. Topalov, Q. Van Overmeere, S. Cherevko, X. Chen, E. Ventosa, W. Schuhmann, K. J. J. Mayrhofer, *RSC Adv.* **2014**, *4*, 9579; b) A. R. Zeradjanin, N. Menzel, P. Strasser, W. Schuhmann, *ChemSusChem* **2012**, *5*, 1897.

[16] Michael E. G Lyons, M. P. Brandon, *Int. J. Electrochem. Sci.* **2008**, *3*, 1463.

[17] N. H. Chou, P. N. Ross, A. T. Bell, T. D. Tilley, *ChemSusChem* **2011**, *4*, 1566.

[18] K. Juodkazis, J. Juodkazytė, R. Vilkauskaitė, V. Jasulaitienė, *J. Solid State Electrochem.* **2008**, *12*, 1469.

[19] Y. Shi, Y. Yu, Y. Liang, Y. Du, B. Zhang, *Angew. Chem., Int. Ed.* **2019**, *58*, 3769.

[20] W. Li, S. Watzele, H. A. El-Sayed, Y. Liang, G. Kieslich, A. S. Bandarenka, K. Rodewald, B. Rieger, R. A. Fischer, *J. Am. Chem. Soc.* **2019**, *141*, 5926.

[21] W. Chen, Y. Liu, Y. Li, J. Sun, Y. Qiu, C. Liu, G. Zhou, Y. Cui, *Nano Lett.* **2016**, *16*, 7588.

[22] a) X. Xu, F. Song, X. Hu, *Nat. Commun.* **2016**, *7*, 12324; b) A. Sivanantham, S. Shanmugam, *Appl. Catal., B* **2017**, *203*, 485; c) J. Zhang, T. Wang, D. Pohl, B. Rellinghaus, R. Dong, S. Liu, X. Zhuang, X. Feng, *Angew. Chem.* **2016**, *128*, 6814; d) Y. Huang, X. Chong, C. Liu, Y. Liang, B. Zhang, *Angew. Chem., Int. Ed.* **2018**, *57*, 13163.

[23] K. Fan, H. Zou, Y. Lu, H. Chen, F. Li, J. Liu, L. Sun, L. Tong, M. F. Toney, M. Sui, J. Yu, *ACS Nano* **2018**, *12*, 12369.

[24] W. Chen, H. Wang, Y. Li, Y. Liu, J. Sun, S. Lee, J. S. Lee, Y. Cui, *ACS Cent. Sci.* **2015**, *1*, 244.

[25] G. Zhang, Y.-S. Feng, W.-T. Lu, D. He, C.-Y. Wang, Y.-K. Li, X.-Y. Wang, F.-F. Cao, *ACS Catal.* **2018**, *8*, 5431.

[26] W. Zhou, X.-J. Wu, X. Cao, X. Huang, C. Tan, J. Tian, H. Liu, J. Wang, H. Zhang, *Energy Environ. Sci.* **2013**, *6*, 2921.

[27] W. Zhu, X. Yue, W. Zhang, S. Yu, Y. Zhang, J. Wang, J. Wang, *Chem. Commun.* **2016**, *52*, 1486.

[28] Y. Wu, Y. Liu, G.-D. Li, X. Zou, X. Lian, D. Wang, L. Sun, T. Asefa, X. Zou, *Nano Energy* **2017**, *35*, 161.

[29] H. Zou, B. He, P. Kuang, J. Yu, K. Fan, *ACS Appl. Mater. Interfaces* **2018**, *10*, 22311.

[30] a) X. Wu, D. He, H. Zhang, H. Li, Z. Li, B. Yang, Z. Lin, L. Lei, X. Zhang, *Int. J. Hydrogen Energy* **2016**, *41*, 10688; b) J. Li, D. Fan, M. Wang, Z. Wang, Z. Liu, K. Zhao, L. Zhou, L. Mai, *ChemElectroChem* **2019**, *6*, 331.

ADVANCED
SCIENCE NEWS
www.advancedsciencenews.com

NANO · MICRO
small
www.small-journal.com

[31] C. Tang, N. Cheng, Z. Pu, W. Xing, X. Sun, *Angew. Chem., Int. Ed.* **2015**, *54*, 9351.

[32] C. Tang, A. M. Asiri, X. Sun, *Chem. Commun.* **2016**, *52*, 4529.

[33] O. Mabayoje, A. Shoola, B. R. Wygant, C. B. Mullins, *ACS Energy Lett.* **2016**, *1*, 195.

[34] Z. Wang, J. Li, X. Tian, X. Wang, Y. Yu, K. A. Owusu, L. He, L. Mai, *ACS Appl. Mater. Interfaces* **2016**, *8*, 19386.

[35] C. Xia, Q. Jiang, C. Zhao, M. N. Hedhili, H. N. Alshareef, *Adv. Mater.* **2016**, *28*, 77.

[36] K. Xu, H. Ding, K. Jia, X. Lu, P. Chen, T. Zhou, H. Cheng, S. Liu, C. Wu, Y. Xie, *Angew. Chem., Int. Ed.* **2016**, *55*, 1710.

[37] I. H. Kwak, H. S. Im, D. M. Jang, Y. W. Kim, K. Park, Y. R. Lim, E. H. Cha, J. Park, *ACS Appl. Mater. Interfaces* **2016**, *8*, 5327.

[38] H. Han, K. M. Kim, H. Choi, G. Ali, K. Y. Chung, Y.-R. Hong, J. Choi, J. Kwon, S. W. Lee, J. W. Lee, J. H. Ryu, T. Song, S. Mhin, *ACS Catal.* **2018**, *8*, 4091.

[39] D. Liu, Q. Lu, Y. Luo, X. Sun, A. M. Asiri, *Nanoscale* **2015**, *7*, 15122.

[40] a) P. Chen, K. Xu, Z. Fang, Y. Tong, J. Wu, X. Lu, X. Peng, H. Ding, C. Wu, Y. Xie, *Angew. Chem., Int. Ed.* **2015**, *54*, 14710; b) J.-H. Kim, K. Kawashima, B. R. Wygant, O. Mabayoje, Y. Liu, J. H. Wang, C. B. Mullins, *ACS Appl. Energy Mater.* **2018**, *1*, 5145.

[41] a) Z. Liu, J. Zhang, Y. Liu, W. Zhu, X. Zhang, Q. Wang, *ChemElectroChem* **2018**, *5*, 1677; b) R. Guo, X. Lai, J. Huang, X. Du, Y. Yan, Y. Sun, G. Zou, J. Xiong, *ChemElectroChem* **2018**, *5*, 3822; c) J. Huang, Y. Sun, Y. Zhang, G. Zou, C. Yan, S. Cong, T. Lei, X. Dai, J. Guo, R. Lu, Y. Li, J. Xiong, *Adv. Mater.* **2018**, *30*, 1705045; d) K. Xu, H. Cheng, L. Liu, H. Lv, X. Wu, C. Wu, Y. Xie, *Nano Lett.* **2017**, *17*, 578; e) F. Yu, H. Zhou, Z. Zhu, J. Sun, R. He, J. Bao, S. Chen, Z. Ren, *ACS Catal.* **2017**, *7*, 2052.

[42] a) J. Huang, Y. Li, Y. Xia, J. Zhu, Q. Yi, H. Wang, J. Xiong, Y. Sun, G. Zou, *Nano Res.* **2017**, *10*, 1010; b) B. You, N. Jiang, M. Sheng, M. W. Bhushan, Y. Sun, *ACS Catal.* **2016**, *6*, 714; c) P. Jiang, Q. Liu, Y. Liang, J. Tian, A. M. Asiri, X. Sun, *Angew. Chem., Int. Ed.* **2014**, *53*, 12855; d) L. Yu, H. Zhou, J. Sun, I. K. Mishra, D. Luo, F. Yu, Y. Yu, S. Chen, Z. Ren, *J. Mater. Chem. A* **2018**, *6*, 13619; e) J. Chang, Y. Xiao, M. Xiao, J. Ge, C. Liu, W. Xing, *ACS Catal.* **2015**, *5*, 6874.

[43] X. Xiao, C.-T. He, S. Zhao, J. Li, W. Lin, Z. Yuan, Q. Zhang, S. Wang, L. Dai, D. Yu, *Energy Environ. Sci.* **2017**, *10*, 893.

[44] a) J. Huang, Y. Sun, X. Du, Y. Zhang, C. Wu, C. Yan, Y. Yan, G. Zou, W. Wu, R. Lu, Y. Li, J. Xiong, *Adv. Mater.* **2018**, *30*, 1803367; b) H. Zhou, F. Yu, J. Sun, R. He, S. Chen, C. W. Chu, Z. Ren, *Proc. Natl. Acad. Sci. USA* **2017**, *114*, 5607.

[45] J. Ryu, N. Jung, J. H. Jang, H.-J. Kim, S. J. Yoo, *ACS Catal.* **2015**, *5*, 4066.

[46] X.-Y. Yu, Y. Feng, B. Guan, X. W. Lou, U. Paik, *Energy Environ. Sci.* **2016**, *9*, 1246.

[47] L.-A. Stern, L. Feng, F. Song, X. Hu, *Energy Environ. Sci.* **2015**, *8*, 2347.

[48] X. Wang, W. Li, D. Xiong, L. Liu, *J. Mater. Chem. A* **2016**, *4*, 5639.

[49] Y. Zhang, B. Ouyang, J. Xu, G. Jia, S. Chen, R. S. Rawat, H. J. Fan, *Angew. Chem., Int. Ed.* **2016**, *55*, 8670.

[50] P. Chen, K. Xu, Y. Tong, X. Li, S. Tao, Z. Fang, W. Chu, X. Wu, C. Wu, *Inorg. Chem. Front.* **2016**, *3*, 236.

[51] C. Walter, P. W. Menezes, S. Orthmann, J. Schuch, P. Connor, B. Kaiser, M. Lerch, M. Driess, *Angew. Chem., Int. Ed.* **2018**, *57*, 698.

[52] J. Wang, W. Cui, Q. Liu, Z. Xing, A. M. Asiri, X Sun, *Adv. Mater.* **2016**, *28*, 215.

[53] T. Zhou, Y. Du, D. Wang, S. Yin, W. Tu, Z. Chen, A. Borgna, R. Xu, *ACS Catal.* **2017**, *7*, 6000.

[54] Y. Li, C. Zhao, *Chem. Mater.* **2016**, *28*, 5659.

[55] J. Xu, J. Li, D. Xiong, B. Zhang, Y. Liu, K. H. Wu, I. Amorim, W. Li, L. Liu, *Chem. Sci.* **2018**, *9*, 3470.

[56] a) W. Xi, G. Yan, Z. Lang, Y. Ma, H. Tan, H. Zhu, Y. Wang, Y. Li, *Small* **2018**, *14*, 1802204; b) Y. Zhan, M. Lu, S. Yang, Z. Liu, J. Y. Lee, *ChemElectroChem* **2016**, *3*, 615; c) L. Yu, I. K. Mishra, Y. Xie,

H. Zhou, J. Sun, J. Zhou, Y. Ni, D. Luo, F. Yu, Y. Yu, S. Chen, Z. Ren, *Nano Energy* **2018**, *53*, 492; d) D. Li, H. Baydoun, C. N. Verani, S. L. Brock, *J. Am. Chem. Soc.* **2016**, *138*, 4006.

[57] K. Xu, P. Chen, X. Li, Y. Tong, H. Ding, X. Wu, W. Chu, Z. Peng, C. Wu, Y. Xie, *J. Am. Chem. Soc.* **2015**, *137*, 4119.

[58] H. S. Ahn, A. J. Bard, *J. Am. Chem. Soc.* **2015**, *137*, 612.

[59] H. Wang, Y. Cao, C. Sun, G. Zou, J. Huang, X. Kuai, J. Zhao, L. Gao, *ChemSusChem* **2017**, *10*, 3540.

[60] a) Y. N. Regmi, C. Wan, K. D. Duffee, B. M. Leonard, *ChemCatChem* **2015**, *7*, 3911; b) J. Xing, Y. Li, S. Guo, T. Jin, H. Li, Y. Wang, L. Jiao, *Electrochim. Acta* **2019**, *298*, 305.

[61] D. Das, S. Santra, K. K. Nanda, *ACS Appl. Mater. Interfaces* **2018**, *10*, 35025.

[62] M. Kim, S. Kim, D. Song, S. Oh, K. J. Chang, E. Cho, *Appl. Catal., B* **2018**, *227*, 340.

[63] Y. Jin, H. Wang, J. Li, X. Yue, Y. Han, P. K. Shen, Y. Cui, *Adv. Mater.* **2016**, *28*, 3785.

[64] X. Leng, K.-H. Wu, B.-J. Su, L.-Y. Jang, I. R. Gentle, D.-W. Wang, *Chin. J. Catal.* **2017**, *38*, 1021.

[65] J. Masa, P. Weide, D. Peeters, I. Sinev, W. Xia, Z. Sun, C. Somsen, M. Muhler, W. Schuhmann, *Adv. Energy Mater.* **2016**, *6*, 1502313.

[66] a) J. Masa, C. Andronescu, H. Antoni, I. Sinev, S. Seisel, K. Elumeeva, S. Barwe, S. Marti-Sanchez, J. Arbiol, B. Roldan Cuenya, M. Muhler, W. Schuhmann, *ChemElectroChem* **2019**, *6*, 235; b) W. Yuan, X. Zhao, W. Hao, J. Li, L. Wang, X. Ma, Y. Guo, *ChemElectroChem* **2019**, *6*, 764; c) N. Xu, G. Cao, Z. Chen, Q. Kang, H. Dai, P. Wang, *J. Mater. Chem. A* **2017**, *5*, 12379; d) Osaka Tetsuya, Iwase Yoshio, Kitayama Hiroshi, I. Toshihiro, *Bull. Chem. Soc. Jpn.* **1983**, *56*, 2106.

[67] H. Li, P. Wen, Q. Li, C. Dun, J. Xing, C. Lu, S. Adhikari, L. Jiang, D. L. Carroll, S. M. Geyer, *Adv. Energy Mater.* **2017**, *7*, 1700513.

[68] X. Ma, J. Wen, S. Zhang, H. Yuan, K. Li, F. Yan, X. Zhang, Y. Chen, *ACS Sustainable Chem. Eng.* **2017**, *5*, 10266.

[69] G. Liu, D. He, R. Yao, Y. Zhao, J. Li, *Nano Res.* **2018**, *11*, 1664.

[70] a) D. K. Bediako, Y. Surendranath, D. G. Nocera, *J. Am. Chem. Soc.* **2013**, *135*, 3662; b) M. Dinca, Y. Surendranath, D. G. Nocera, *Proc. Natl. Acad. Sci. USA* **2010**, *107*, 10337; c) D. K. Bediako, B. Lassalle-Kaiser, Y. Surendranath, J. Yano, V. K. Yachandra, D. G. Nocera, *J. Am. Chem. Soc.* **2012**, *134*, 6801.

[71] M. Yoshida, Y. Mitsutomi, T. Mineo, M. Nagasaka, H. Yuzawa, N. Kosugi, H. Kondoh, *J. Phys. Chem. C* **2015**, *119*, 19279.

[72] B. Ewald, Y.-X. Huang, R. Kniep, *Z. Anorg. Allg. Chem.* **2007**, *633*, 1517.

[73] P. W. Menezes, A. Indra, I. Zaharieva, C. Walter, S. Loos, S. Hoffmann, R. Schlögl, H. Dau, M. Driess, *Energy Environ. Sci.* **2019**, *12*, 988.

[74] a) M. Gao, W. Sheng, Z. Zhuang, Q. Fang, S. Gu, J. Jiang, Y. Yan, *J. Am. Chem. Soc.* **2014**, *136*, 7077; b) J. Xie, X. Zhang, H. Zhang, J. Zhang, S. Li, R. Wang, B. Pan, Y. Xie, *Adv. Mater.* **2017**, *29*, 1604765.

[75] Q. He, Y. Wan, H. Jiang, Z. Pan, C. Wu, M. Wang, X. Wu, B. Ye, P. M. Ajayan, L. Song, *ACS Energy Lett.* **2018**, *3*, 1373.

[76] B. Zhang, K. Jiang, H. Wang, S. Hu, *Nano Lett.* **2019**, *19*, 530.

[77] Z. Chen, L. Cai, X. Yang, C. Kronawitter, L. Guo, S. Shen, B. E. Koel, *ACS Catal.* **2018**, *8*, 1238.

[78] J. Zhang, J. Liu, L. Xi, Y. Yu, N. Chen, S. Sun, W. Wang, K. M. Lange, B. Zhang, *J. Am. Chem. Soc.* **2018**, *140*, 3876.

[79] M. B. Stevens, C. D. M. Trang, L. J. Enman, J. Deng, S. W. Boettcher, *J. Am. Chem. Soc.* **2017**, *139*, 11361.

[80] K. Izumiya, E. Akiyama, H. Habazaki, A. Kawashima, K. Asami, K. Hashimoto, *J. Appl. Electrochem.* **1997**, *27*, 1362.

[81] B. S. Yeo, A. T. Bell, *J. Am. Chem. Soc.* **2011**, *133*, 5587.

[82] a) A. Bergmann, E. Martinez-Moreno, D. Teschner, P. Chernev, M. Gliech, J. F. de Araujo, T. Reier, H. Dau, P. Strasser,

**ADVANCED
SCIENCE NEWS**

www.advancedsciencenews.com

**NANO · MICRO
small**

www.small-journal.com

Nat. Commun. **2015**, *6*, 8625; b) C.-W. Tung, Y.-Y. Hsu, Y.-P. Shen, Y. Zheng, T.-S. Chan, H.-S. Sheu, Y.-C. Cheng, H. M. Chen, *Nat. Commun.* **2015**, *6*, 8106.

[83] H. Y. Wang, Y. Y. Hsu, R. Chen, T. S. Chan, H. M. Chen, B. Liu, *Adv. Energy Mater.* **2015**, *5*, 1500091.

[84] Y. Duan, S. Sun, Y. Sun, S. Xi, X. Chi, Q. Zhang, X. Ren, J. Wang, S. J. H. Ong, Y. Du, L. Gu, A. Grimaud, Z. J. Xu, *Adv. Mater.* **2019**, *31*, 1807898.

[85] K. J. May, *Masters Thesis,* Massachusetts Institute of Technology **2013**.

[86] E. Fabbri, M. Nachtegaal, T. Binninger, X. Cheng, B. J. Kim, J. Durst, F. Bozza, T. Graule, R. Schaublin, L. Wiles, M. Pertoso, N. Danilovic, K. E. Ayers, T. J. Schmidt, *Nat. Mater.* **2017**, *16*, 925.

[87] Y. Zhu, W. Zhou, J. Sunarso, Y. Zhong, Z. Shao, *Adv. Funct. Mater.* **2016**, *26*, 5862.

[88] B. J. Kim, E. Fabbri, D. F. Abbott, X. Cheng, A. H. Clark, M. Nachtegaal, M. Borlaf, I. E. Castelli, T. Graule, T. J. Schmidt, *J. Am. Chem. Soc.* **2019**, *141*, 5231.

[89] a) X. Xu, Y. Chen, W. Zhou, Y. Zhong, D. Guan, Z. Shao, *Adv. Mater. Interfaces* **2018**, *5*, 1701693; b) X. Xu, W. Wang, W. Zhou, Z. Shao, *Small Methods* **2018**, *2*, 1800071; c) X. Xu, C. Su, W. Zhou, Y. Zhu, Y. Chen, Z. Shao, *Adv. Sci.* **2016**, *3*, 1500187; d) R. Ignatans, G. Mallia, E. A. Ahmad, L. Spillane, K. A. Stoerzinger, Y. Shao-Horn, N. M. Harrison, V. Tileli, *J. Phys. Chem. C* **2019**, *123*, 11621.

[90] X. Zheng, B. Zhang, P. De Luna, Y. Liang, R. Comin, O. Voznyy, L. Han, F. P. Garcia de Arquer, M. Liu, C. T. Dinh, T. Regier, J. J. Dynes, S. He, H. L. Xin, H. Peng, D. Prendergast, X. Du, E. H. Sargent, *Nat. Chem.* **2018**, *10*, 149.